



## Abstract

In the recent chemistry version (v3.3) of the Weather Research and Forecasting (WRF-Chem) model, we have coupled the Morrison double-moment microphysics scheme with interactive aerosols so that two-way aerosol-cloud interactions are included in the simulations. We have used this new WRF-Chem functionality in a study focused on assessing predictions of aerosols, marine stratocumulus clouds, and their interactions over the Southeast Pacific using measurements from the VAMOS Ocean-Cloud-Atmosphere-Land Study Regional Experiment (VOCALS-REx) and satellite retrievals. This study also serves as a detailed analysis of our WRF-Chem simulations contributed to the VOCALS model Assessment (VOCA) project. The WRF-Chem 31-day (15 October–16 November 2008) simulation with aerosol-cloud interactions (AERO hereafter) is also compared to a simulation (MET hereafter) with fixed cloud droplet number concentrations assumed by the default in Morrison microphysics scheme with no interactive aerosols. The well-predicted aerosol properties such as number, mass composition, and optical depth lead to significant improvements in many features of the simulated stratocumulus clouds: cloud optical properties and microphysical properties such as cloud top effective radius, cloud water path, and cloud optical thickness, and cloud macrostructure such as cloud depth and cloud base height. In addition to accounting for the aerosol direct and semi-direct effects, these improvements feed back to the prediction of boundary-layer characteristics and energy budgets. Particularly, inclusion of interactive aerosols in AERO strengthens the temperature and humidity gradients within the capping inversion layer and lowers the marine boundary layer depth by 150 m from that of the MET simulation. Mean top-of-the-atmosphere outgoing short-wave fluxes, surface latent heat, and surface downwelling longwave fluxes are in better agreement with observations in AERO, compared to the MET simulation. Nevertheless, biases in some of the simulated meteorological quantities (e.g., MBL temperature and humidity over the remote ocean) and aerosol quantities (e.g., overestimations of supermicron sea salt mass) might affect simulated stratocumulus and energy fluxes

## Assessing regional scale predictions of marine stratocumulus

Q. Yang et al.

Title Page

Abstract

Introduction

Conclusions

References

Tables

Figures



Back

Close

Full Screen / Esc

Printer-friendly Version

Interactive Discussion



over the southeastern Pacific Ocean, and require further investigations. Although not perfect, the overall performance of the regional model in simulating mesoscale aerosol-cloud interactions is encouraging and suggests that the inclusion of spatially varying aerosol characteristics is important when simulating marine stratocumulus over the southeastern Pacific.

## 1 Introduction

Marine stratocumuli play an important role in radiation and hydrological budgets, particularly along the eastern edges of oceans, such as over the Southeast Pacific (SEP) (Stevens et al., 2005; Stevens and Feingold, 2009). These clouds are bright compared to the dark ocean surface and result in much more shortwave scattered back to space. Their effective temperature is comparable to that of the ocean surface, so the emitted longwave radiation imposes little compensating effect. Therefore, properly representing these clouds in climate models is important. However, marine stratocumuli are notoriously difficult to model accurately. The recent Preliminary VOCALS model Assessment (PreVOCA) (Wyant et al., 2010) showed a wide range in behavior among models in representing such clouds. One reason for this difference is the simplified approach to aerosols used by most models, where a constant background aerosol concentration or cloud droplet number concentration is assumed in the microphysics modules. In reality, strong gradients in aerosol number and speciation exist as one progresses westward from the coast of South America towards the open ocean. These gradients result in cloud condensation nuclei (CCN) gradients and lead to differing cloud characteristics as well.

Reproducing CCN gradients is important to properly simulate the marine stratocumulus over the SEP. This paper shows the improvement gained in using an interactive aerosol-cloud module in the chemistry version of the Weather Research and Forecasting (WRF-Chem) model (Grell et al., 2005; Fast et al., 2006). Specifically, a new coupling between the double-moment Morrison microphysics scheme (Morrison et al.,

## Assessing regional scale predictions of marine stratocumulus

Q. Yang et al.

Title Page

Abstract

Introduction

Conclusions

References

Tables

Figures

⏪

⏩

◀

▶

Back

Close

Full Screen / Esc

Printer-friendly Version

Interactive Discussion



## Assessing regional scale predictions of marine stratocumulus

Q. Yang et al.

Title Page

Abstract

Introduction

Conclusions

References

Tables

Figures

⏪

⏩

◀

▶

Back

Close

Full Screen / Esc

Printer-friendly Version

Interactive Discussion

2008) and aerosol modules is used; we implemented this coupling in the April 2011 v3.3 release of WRF-Chem. The VAMOS Ocean-Cloud-Atmosphere-Land Study Regional Experiment (VOCALS-REx) was a field campaign during October and November 2008 designed to improve the scientific understanding of model simulations and predictions of the coupled climate system over the SEP (Wood et al., 2011b). The campaign provided extensive measurements for evaluating the capability of our model with the aforementioned new coupling in predicting aerosol and marine stratus clouds over this region.

A recent modeling exercise conducted by Abel et al. (2010) with the UK Met Office Unified Model (MetUM) is parallel to this model evaluation study. MetUM simulated a good representation of synoptically induced variability in cloud cover and boundary layer depth during the VOCALS-REx (Abel et al., 2010). However, the exclusion of cloud-aerosol interactions and the model's relatively simple parameterization of cloud-microphysical effects (Tonizzzo et al., 2011) precluded better agreement with field observations.

Aerosol-cloud interactions are important to the variability of marine stratus. Aerosols can impact radiative fluxes directly through absorption and scattering (the direct effect), and indirectly through their impact on liquid clouds via the so-called indirect effects (Twomey, 1977; Albrecht, 1989). The first indirect effect is the change in cloud albedo due to the change in cloud droplet number and radius. The second indirect effect (also known as the 'cloud lifetime effect') is the change in cloud lifetime and precipitation due to change in cloud droplet number; the importance of this second indirect effect on radiative forcing is also evident in shallow marine stratus (Stevens and Feingold, 2009). By changing warm-rain processes in marine stratocumulus clouds, aerosols can alter cloud cellular structures and boundary-layer mesoscale circulations in ways that are much more complicated than traditionally depicted by conceptual models of the indirect effects (Steven et al., 2005; Wang and Feingold, 2009a, b). The emerging importance and complexity of aerosol-cloud-precipitation interactions in shallow marine stratus is gaining recognition by the scientific community (Stevens and Feingold, 2009).

These aerosol-cloud interactions and dynamical feedbacks are particularly important over the SEP.

Strong gradients of anthropogenic and natural aerosols in the marine boundary layer (MBL), make the SEP an ideal location for studying the response of shallow marine clouds to aerosol perturbations. Along the coast of Chile and Peru, copper smelters, power plants, and oil refineries emit large amounts of oxidized sulfur (sulfur dioxide (SO<sub>2</sub>) + sulfate) (Huneeus et al., 2006). Other continental sources include volcanic, biomass burning, biogenic, and dust emissions. Associated with mid-latitude synoptic-scale disturbances, the emitted trace gases and particles over the continent can reach the stratus deck when blown by the frequent easterly winds which subside down the subtropical Andes in Northern Chile (Huneeus et al., 2006). These continental pollutants, both primary and secondary, then are mixed with trace gases and particles from oceanic emissions. Marine sources of primary aerosols include sea-salt and organic compounds from sea spray and bubble bursting (Russell et al., 2010), and a source of secondary aerosols is the oxidation of dimethyl sulfide (DMS) to sulfate. Detailed understanding of the aerosol-cloud interactions (e.g., the transition from closed to open cellular convection) and properly reproducing the climate impact of these clouds remain a challenge for current climate modeling.

This study evaluates simulated aerosols and cloud fields in the WRF-Chem model with the newly implemented coupling between the double-moment Morrison microphysics scheme and aerosols, and is a necessary first step before progressing to further studies on multiple aerosol-cloud equilibrium regimes and the sensitivity of predicted SEP cloud fields to model horizontal grid resolution. A simulation with spatially and temporally varying aerosols is compared against another with the default configuration of the Morrison scheme, which assumes a fixed cloud droplet number concentration. A description of the model and observational data is provided in Sect. 2. In Sect. 3, we first discuss the characteristics of the simulated marine boundary layer (Sect. 3.1), then evaluate simulated aerosol (Sect. 3.2), cloud optical properties (Sect. 3.3) and cloud macro structures (Sect. 3.4). The domain-average top-of-the-atmosphere (TOA)

**Assessing regional scale predictions of marine stratocumulus**

Q. Yang et al.

Title Page

Abstract

Introduction

Conclusions

References

Tables

Figures



Back

Close

Full Screen / Esc

Printer-friendly Version

Interactive Discussion



shortwave (SW) fluxes and longitudinal and diurnal variations in surface energy fluxes are discussed in Sect. 3.5. Model representations of longitudinal and vertical variations of drizzle are shown in Sect. 3.6. The discussion and summary of the evaluation results are presented in Sects. 4 and 5, respectively.

## 2 Model Description and Observational Data

### 2.1 WRF-Chem

WRF-Chem is a widely used regional model employed operationally for air quality (e.g., Zhang et al., 2010) and tracer forecasting (<http://www-frd.fsl.noaa.gov/aq/wrf/>), detailed aerosol process studies (e.g., Fast et al., 2009), and regional climate studies involving aerosols (e.g., Qian et al., 2009). It includes full online interactions between aerosols, radiation, and clouds for the direct, semi-direct, and first and second indirect effects as described in Fast et al. (2006), Chapman et al. (2009), and Gustafson et al. (2007). Past research included aerosol indirect effects only through the Lin microphysics scheme. This has now been complemented in WRF-Chem v3.3 with the additional option to use the Morrison microphysics scheme. The simulations presented in this study were performed by using the code as implemented in WRF-Chem v3.2.1, which was then released to the public in v3.3.

Table 1 shows the model configuration used for the simulations in this study. The configuration is standard for simulations involving full aerosol-climate effects. The Model for Simulating Aerosol Interactions and Chemistry (MOSAIC) (Zaveri et al., 2008) is implemented with a sectional approach where the size distributions for both unactivated/interstitial and cloud-borne aerosols are represented with 8 bins. The bin sizes defined by their lower and upper dry particle diameters are provided in Table 2. What is new compared to previous published studies using the MOSAIC aerosol module is the inclusion of DMS chemistry as a source of atmospheric SO<sub>2</sub> and sulfuric acid (H<sub>2</sub>SO<sub>4</sub>). In this study, a correction has been made to the reaction rate for the decomposition of

## Assessing regional scale predictions of marine stratocumulus

Q. Yang et al.

Title Page

Abstract

Introduction

Conclusions

References

Tables

Figures

⏪

⏩

◀

▶

Back

Close

Full Screen / Esc

Printer-friendly Version

Interactive Discussion



methanesulfonyl ( $\text{CH}_3\text{SO}_2$ ) radicals into  $\text{SO}_2$ , which has been incorporated into WRF-Chem v3.3. Secondary organic aerosol formation (Shrivastava et al., 2010) is not included in the simulations presented here to reduce the overall computational expense and, as shown later, organic aerosols are a relatively small fraction of the total aerosol mass over the SEP.

The Morrison microphysics scheme predicts changes of number and mass mixing ratios of cloud water, cloud ice, snow, rain, and graupel/hail associated with the following microphysics processes: autoconversion (transfer of mass and number concentration from the cloud ice and droplet classes to snow and rain due to coalescence and diffusional growth), collection between hydrometeor species, melting/freezing, and ice multiplication (transfer of mass from snow to ice) (Morrison and Pinto, 2005). Cloud droplets are represented by a gamma distribution and the size distributions of all other hydrometeor species are assumed to follow an exponential function (Morrison et al., 2009). When interactive aerosols are not included, a constant droplet concentration of  $250\text{ cm}^{-3}$  is assumed. The activation and more complex couplings with interactive aerosols are described as follows. Activation of aerosols to cloud droplets is based on the maximum supersaturation, which is diagnosed using a combination of the resolved vertical velocity and turbulent motions in combination with the internally mixed aerosol properties within each size bin (Chapman et al., 2009). Aerosol and cloud interactions in warm clouds occur in two ways: aerosols affect clouds (activation of CCN is the main source of cloud droplets) and clouds affect aerosols (wet removal is the main sink of submicron particles and cloud chemistry is a major source of sulfate). The interactions of clouds and shortwave radiation for the first indirect effect are implemented by linking the predicted cloud droplet number from the Morrison microphysics scheme with the Goddard shortwave radiative scheme. The second indirect effect is handled directly by the microphysics scheme for warm-rain processes, where the number of activated particles affects cloud precipitation and lifetime. Aerosol effects on longwave radiation are not included in this study, but have also been recently incorporated into WRF v3.3 as described in Zhao et al. (2010).

## Assessing regional scale predictions of marine stratocumulus

Q. Yang et al.

[Title Page](#)[Abstract](#)[Introduction](#)[Conclusions](#)[References](#)[Tables](#)[Figures](#)[⏪](#)[⏩](#)[◀](#)[▶](#)[Back](#)[Close](#)[Full Screen / Esc](#)[Printer-friendly Version](#)[Interactive Discussion](#)

## Assessing regional scale predictions of marine stratocumulus

Q. Yang et al.

Title Page

Abstract

Introduction

Conclusions

References

Tables

Figures

⏪

⏩

◀

▶

Back

Close

Full Screen / Esc

Printer-friendly Version

Interactive Discussion



Scalar advection was found to be critical to the performance of a double-moment microphysics scheme incorporated into WRF when simulating stratocumulus clouds with interactive CCN, particularly near strong gradients (Wang et al., 2009); therefore, we employ the monotonic advection scheme for model scalars and chemical species for better accuracy in advection even though it is more computationally expensive.

Simulated evolution of the MBL and stratocumulus clouds will be highly dependent upon the Planetary Boundary Layer (PBL) parameterization with our 9 km horizontal grid spacing. In this study, the YSU scheme (Hong et al., 2006) is used that employs a nonlocal-K (vertical diffusion coefficient) mixing for momentum, entrainment of heat and momentum fluxes at the PBL top, a local K approach for atmospheric diffusion above the mixed layer, and a critical bulk Richardson number of zero for the PBL top.

The model domain covers part of the northern Chilean and southern Peruvian coasts and the nearby Southeast Pacific, roughly 63° W–93° W in longitude and 11° S–36° S in latitude. Throughout the paper, two regions, the “coastal region” and the “remote region”, are defined. The two regions are separated by the 78° W meridian with the west (remote region) characterized by more remote marine aerosol conditions and the east (coastal region) characterized by anthropogenic influences mixed with the maritime background. From the surface to 50 hPa, the model has 64 vertical layers, and the layer thickness increases from ~30 m at the surface to ~50 m at 1 km and ~90 m at 2 km above the ocean surface. The horizontal grid spacing is 9 km. Excluding five-days of model spin up, the simulation period is from 00:00 UTC 15 October 2008 to 00:00 UTC 16 November 2008. Initial conditions, boundary conditions, and time dependent sea surface temperatures (SSTs) for meteorology were obtained from the Global Forecast System (GFS) model output with a 0.5-degree grid spacing, while the Model for Ozone and Related chemical Tracers (MOZART) provided the initial and boundary conditions for trace gases and aerosols. For comparison purposes, two simulations were conducted: one simulation with aerosol-cloud interactions (referred to as AERO) and the other simulation with aerosol and chemistry modules turned off and droplet number prescribed (referred to as MET).

## Assessing regional scale predictions of marine stratocumulus

Q. Yang et al.

Title Page

Abstract

Introduction

Conclusions

References

Tables

Figures

⏪

⏩

◀

▶

Back

Close

Full Screen / Esc

Printer-friendly Version

Interactive Discussion



Emissions used for the AERO simulation are as follows. Coarse and fine mode sea-salt emissions are based on Gong et al. (1997) and Monahan et al. (1986), which neglect sea-salt production through breaking waves, while ultrafine sea-salt emissions follow Clarke et al. (2006). Sea-salt particles are treated as NaCl in the model.

DMS emissions are calculated using a simplified Nightingale et al. (2000) scheme with constant SST and a geographically uniform ocean surface DMS concentration of  $2.8 \text{ nML}^{-1}$  as specified in the VOCA Modeling Experiment Specification ([http://www.atmos.washington.edu/~mwyant/vocals/model/VOCA\\_Model\\_Spec.htm](http://www.atmos.washington.edu/~mwyant/vocals/model/VOCA_Model_Spec.htm)). Terrestrial biogenic emissions are calculated using the MEGAN (Guenther et al., 2006) emission module in WRF-Chem. The VOCA Emission inventory compiled by the University of Iowa specifically for VOCA supplied anthropogenic and volcanic emissions. Emissions of carbon monoxide (CO), oxides of nitrogen ( $\text{NO}_x$ ),  $\text{SO}_2$ , ammonia ( $\text{NH}_3$ ), black carbon (BC), organic carbon (OC), particles  $10 \mu\text{m}$  or less in diameter ( $\text{PM}_{10}$ ), particles  $2.5 \mu\text{m}$  or less in diameter ( $\text{PM}_{2.5}$ ), and volatile organic compounds (VOCs) are included in the VOCA inventory; oceanic  $\text{NH}_3$  emissions are not included. Biomass burning emissions (CO,  $\text{NO}_x$ ,  $\text{SO}_2$ ,  $\text{NH}_3$ , VOCs, OC, BC, and  $\text{PM}_{2.5}$ ) are based on the MODerate resolution Imaging Spectroradiometer (MODIS) fire counts and combustion estimates that depend on location-specific vegetation type (Wiedinmyer et al., 2010). Windblown dust emissions are based on the Shaw et al. (2008) formulation.

## 2.2 Observational Data

A wide range of meteorological, trace gas, and aerosol measurements were collected during VOCALS-REx as described in Wood et al. (2011b). Here we briefly describe the observations that are employed in this modeling study. Detailed descriptions of the instruments can be found elsewhere (e.g., Allen et al., 2011; Wood et al., 2011a).

## 2.2.1 Aerosol number and mass concentrations

During the VOCALS-REx, a Particle Measurement System (PMS) Passive Cavity Aerosol Spectrometer Probe (PCASP) measured accumulation mode aerosol particles (dry diameter 0.117–2.94  $\mu\text{m}$ ) on the NCAR C-130 aircraft. For the purpose of matching aerosol particle sizes between PCASP measurements and model simulations, this study uses only measured aerosol particle concentrations with diameters of 0.156–2.69  $\mu\text{m}$ .

Aerosol Mass Spectrometers (AMS) described below measured non-refractory, non sea-salt mass loading of sulfate, ammonium, nitrate, and particulate organic matter (OM). The AMS on the C-130 aircraft (DeCarlo et al., 2006) measured aerosol components aloft for particle sizes (vacuum aerodynamic diameter) between 0.05 and 0.5  $\mu\text{m}$  and the AMS on the G-1 aircraft (Kleinman et al., 2011) measured aerosol compositions in the 0.06–0.6  $\mu\text{m}$  diameter range. The AMS onboard the NOAA R/V Ronald H. Brown research vessel (hereafter RB) provided surface-level particle measurements in the submicron range.

The sub- and supermicron chloride and sodium aerosols were sampled by two-stage multi-jet cascade impactors (CI) on the RB, with 50 % aerodynamic cutoff diameters of 1.1 and 10  $\mu\text{m}$  at <60 % relative humidity. Submicron chloride and sodium were also sampled by a Particle Into Liquid Sampler (PILS) on the G-1 aircraft, with a sampled particle size range of 0.06–1.5  $\mu\text{m}$  at ambient humidity. The samples obtained with both the CI and PILS were analyzed using ion chromatography. Corresponding modeled aerosol concentrations were obtained by first converting the measured particle wet-diameter size range to a dry-diameter size range (using the model's aerosol hygroscopicity), and then integrating the model's aerosol size distribution over this dry-diameter range. For model size bins partially included in the sampling range, a local quadratic fit between logarithmic diameter and mass in adjacent bins was used to estimate the mass in a partial bin.

### Assessing regional scale predictions of marine stratocumulus

Q. Yang et al.

Title Page

Abstract

Introduction

Conclusions

References

Tables

Figures



Back

Close

Full Screen / Esc

Printer-friendly Version

Interactive Discussion



## 2.2.2 Cloud droplet, precipitation sizing data and cloud height

Cloud droplet sizing data measured by a PMS Cloud Droplet Probe (CDP) were available for 12 out of the 14 C-130 flights. This probe measures droplets in diameters of 1–48  $\mu\text{m}$ .

Precipitation sizing data obtained by a PMS 2D-cloud (2D-C) probe on the C-130 were used to derive rain rates. The 2D-C probe measured raindrops in 62.5–1587.5  $\mu\text{m}$  diameter range with 25- $\mu\text{m}$  resolution. Note that excluding smaller size raindrops (<62.5  $\mu\text{m}$ ) could lead to a slight underestimation of the derived rain rates. In calculating rain rates from the measured droplet size distributions, relationships between fall velocities and raindrop diameters were based on Rogers and Yau (1989). Rain rates derived from the 2D-C measurements were then averaged for each 120-s flight leg segment with constant heading and elevation.

Cloud top and cloud base height retrievals were from measurements by the Wyoming cloud radar (WCR) and a upward-pointing lidar (WCL) aboard the C-130 aircraft, respectively.

## 2.2.3 Satellite data

MODIS aerosol and cloud products (Level II Collection 5) were also used to evaluate the WRF-Chem simulations. Compared with ground-based AERONET observations, Collection 5 MODIS aerosol optical depth (AOD) is within the expected accuracy of  $\pm (0.03 + 0.05 \tau)$  for more than 60 % of the time over the ocean, where  $\tau$  is the AOD value (Remer et al., 2008). Both Terra and Aqua satellites have MODIS sensors aboard; however, according to Remer et al. (2008) Terra AOD has an unexpected and unexplained higher value over the ocean. Therefore, we used only MODIS aerosol products from Aqua. To be consistent, we also focused on cloud products from Aqua. In addition, we employed the low-cloud cover products retrieved from the GOES-10 channel 4 infrared radiances as described in Abel et al. (2010), available on a  $0.5^\circ \times 0.5^\circ$  grid,

### Assessing regional scale predictions of marine stratocumulus

Q. Yang et al.

Title Page

Abstract

Introduction

Conclusions

References

Tables

Figures



Back

Close

Full Screen / Esc

Printer-friendly Version

Interactive Discussion



and outgoing shortwave (SW) fluxes measured by the Clouds and the Earth's Radiant Energy System (CERES) aboard Terra (Loeb et al., 2005).

### 3 Model results evaluated against observations

In this section, model simulations are evaluated against measurements from VOCALS-REx and satellite retrievals for the period from 00:00 UTC 15 October 2008 to 00:00 UTC 16 November 2008. Comparisons with aircraft-/ship-based measurements used coincident data; model data were interpolated to the time and location of each measurement datum. Basic statistics, i.e. mean, standard deviation, and median, provided in Tables 3–7 are based on measurements from all available flights and cruises and their corresponding coincident model predictions during the 31-day period for the coastal and remote regions, and for the entire domain. MODIS retrievals were first gridded to the model domain. Then, both the gridded satellite data and the coincident model predictions were averaged over the entire study period for the statistics shown in Tables 3–7.

#### 3.1 Boundary layer structure

Since marine stratocumulus clouds are sensitive to boundary layer conditions, we first evaluate simulated vertical profiles of virtual potential temperature ( $\theta_v$ ) and water vapor mixing ratio ( $q_v$ ) with those observed by radiosondes from the RB (Fig. 1 and Table 3). The observed MBL is more well-mixed over the coastal region than over the remote marine region. As evident in observed profiles over the remote region, there is more frequent decoupling (e.g., Zuidema et al., 2009) within the MBL over the remote region that separates the well-mixed cloud layer from the subcloud layer. The coastal region also has a stronger capping inversion with a 10–12 K increase in  $\theta_v$  and a 5–6 g kg<sup>-1</sup> decrease in  $q_v$  within inversion layers. In addition, the coastal MBL is ~2 K colder and ~2 g kg<sup>-1</sup> less humid, on average, than the remote MBL (Table 3). This humidity

## Assessing regional scale predictions of marine stratocumulus

Q. Yang et al.

Title Page

Abstract

Introduction

Conclusions

References

Tables

Figures



Back

Close

Full Screen / Esc

Printer-friendly Version

Interactive Discussion



contrast was not reported in Bretherton et al. (2010). Systematic differences exist between airborne and balloon humidity sensors, therefore, mixing of data from different sensors in Bretherton et al. (2010) might have obscured this contrast. Temperature and humidity contrasts between coastal and remote regions might be related to cooler SSTs near the coast in addition to differences in cloud characteristics between the two regions.

Differences between AERO and MET in mean profiles of  $\theta_v$  and  $q_v$  are small, except within the simulated inversion layer. In the coastal MBL, mean profiles from both simulations agree quite well with observations (biases of about  $-0.6$  K and  $-0.6$  g kg $^{-1}$ ). Within the coastal inversion layer, errors in the simulated mean temperature and humidity have mean biases of approximately 2 K and 1 g kg $^{-1}$ , respectively. In the coastal free troposphere ( $< 3$  km), the simulated temperature is  $\sim 1$  K lower, while the simulated  $q_v$  is  $\sim 3$  g kg $^{-1}$  higher than observations. Over the remote region, the simulated mean temperature and humidity have biases of approximately  $-2$  to  $-4$  K and  $-1$  g kg $^{-1}$  throughout the MBL and the lower free troposphere.

The AERO and MET simulations both predict an inversion base temperature of approximately 291 K, similar to the observed value over the coastal region, while over the remote region, the inversion base temperature is under-predicted by  $\sim 4$  K ( $\sim 296$  K in observed) by both simulations. As shown in Table 3 and Fig. 1, the AERO simulation better predicts the temperature and humidity gradients within the inversion layer than does the MET over both regions, except for the humidity gradient over the remote region.

As discussed earlier, the MBL further offshore is slightly warmer and more humid compared to the coastal region. This temperature contrast is simulated well in the model, but to a lesser extent than what was observed. The simulated moisture contrast, however, is too small ( $< 0.5$  g kg $^{-1}$ ). The remote region also exhibits greater variability in observations as indicated by the 3–4 times larger standard deviation compared to the coastal region (Table 3 and grey area in Fig. 1). This observed larger variability over the remote region is related to open/closed cellular dynamics. The inability of

## Assessing regional scale predictions of marine stratocumulus

Q. Yang et al.

[Title Page](#)[Abstract](#)[Introduction](#)[Conclusions](#)[References](#)[Tables](#)[Figures](#)[⏪](#)[⏩](#)[◀](#)[▶](#)[Back](#)[Close](#)[Full Screen / Esc](#)[Printer-friendly Version](#)[Interactive Discussion](#)

## Assessing regional scale predictions of marine stratocumulus

Q. Yang et al.

Title Page

Abstract

Introduction

Conclusions

References

Tables

Figures



Back

Close

Full Screen / Esc

Printer-friendly Version

Interactive Discussion



our model to resolve subgrid-size open-cell cumuliform clouds is likely responsible for the simulated small variability in  $\theta_v$  and  $q_v$  over the remote region where open cells are more frequently observed. The larger observed variability could also be linked to larger diurnal variations of cloud cover (shown later) and solar heating, larger variations in surface sensible and latent heat fluxes, and the more active MBL mixing over this region.

The zonal and diurnal variations of predicted MBL depths are compared to those from observations, as shown in Fig. 2 and Table 3. The MBL depth is determined as the lowest height where the local temperature gradient is at least 3 times the gradient below. When a reasonable MBL depth is not found using this approach, the MBL depth is determined from humidity profiles in a similar manner. The clear longitude dependence of observed MBL depths (in the range of 0.7–1.6 km), which deepen farther away from the coast, is also reflected in both AERO and MET simulations (Fig. 2). The MBL depth from the MET simulation has a positive bias of  $\sim 150$  m (Table 3) over the remote region. Inclusion of interactive aerosols in the AERO simulation leads to a lower MBL than in MET, giving better agreement with observations over the remote region (Table 3). However, the mean MBL depth from AERO is approximately 150 m too low over the coastal region. The lower simulated MBL depths when aerosols are included could be due to the reduction of entrainment and turbulent mixing or changes in large-scale dynamics caused by a decrease of the liquid water path (LWP). The WRF simulations described by Rahn and Garreaud (2010) using the Mellor-Yamada-Janjic PBL scheme had lower MBL depths than observations, which is consistent with our results near the coastal region but not over the remote region. This might be due to differences in model setup, including the use of different PBL schemes. As with Rahn and Garreaud (2010), the low bias in the mean MBL depth near the coast in both AERO and MET simulations could be explained by an over-prediction of low-level onshore wind speeds which lead to high biases in low-level divergence over a several hundred meter vertical layer resulting in lowering of MBL heights.

No significant diurnal variations in MBL depth are observed or modeled (bottom panel of Fig. 2). The lack of distinct diurnal variations in MBL depth is consistent with Zuidema et al. (2009) and Rahn and Garreaud (2010) that describe weak dependence of MBL depth on air-sea temperature differences. It is worth noting that the variation during the daytime tends to be larger than that of the nighttime. In addition, there is considerable day-to-day and spatial variability in MBL heights as reflected in standard deviations ( $\sigma = 152$  m for observations;  $\sigma = 214$  m and 276 m for the AERO and MET, respectively).

## 3.2 Aerosol and cloud droplets

### 3.2.1 Aerosol and cloud droplet number concentrations

MBL processes, transport, and anthropogenic and natural aerosol and precursor emissions influence the distribution of aerosol. In this section, we first compare the model simulated and aircraft in-situ measured accumulation mode aerosol number ( $N_a$ , 0.156–2.69  $\mu\text{m}$ , Fig. 3 and Table 3) and cloud droplet number concentrations ( $N_d$ , Fig. 3 and Table 3). Observed aerosol and cloud droplet number concentrations both have strong longitudinal gradients over the coastal region. As shown in Fig. 3, the observed  $N_a$  in the sub-cloud layer (on average 170 m above sea surface) is  $290 \pm 117 \text{ cm}^{-3}$  just west of the coast (71–72° W), decreasing to  $117 \pm 93 \text{ cm}^{-3}$  at ~78° W. The mean observed concentration over the remote region is  $105 \pm 95 \text{ cm}^{-3}$  (Table 3). The modeled  $N_a$  in the sub-cloud layer resembles the observed in longitudinal variation. However, simulated  $N_a$  concentrations (from model size bins 3–6) are lower than observations with mean biases of 34 % and 23 % over the coastal and remote regions, respectively. The predicted size distribution peaks at model size bin 2 (0.08–0.16  $\mu\text{m}$  in diameter), and the number concentration in model size bin 2 is about 1.5 times the modeled  $N_a$  concentration (includes model bins 3–6). Thus, errors in the size distribution could contribute to the number bias. Given the multitude of source and sink processes that affect aerosol number concentrations, the ~30 %  $N_a$  bias is quite good.

22677

## Assessing regional scale predictions of marine stratocumulus

Q. Yang et al.

Title Page

Abstract

Introduction

Conclusions

References

Tables

Figures

⏪

⏩

◀

▶

Back

Close

Full Screen / Esc

Printer-friendly Version

Interactive Discussion



**Assessing regional  
scale predictions of  
marine  
stratocumulus**

Q. Yang et al.

Title Page

Abstract

Introduction

Conclusions

References

Tables

Figures

⏪

⏩

◀

▶

Back

Close

Full Screen / Esc

Printer-friendly Version

Interactive Discussion



Overall, simulated and observed cloud droplet number concentrations exhibit the same longitudinal gradient as that of the aerosol. This is expected, since hygroscopic aerosol particles acting as CCN can activate and form new cloud droplets. The observed  $N_d$  has a value of  $240\text{ cm}^{-3}$  near the coast and decreases to below  $120\text{ cm}^{-3}$  at  $\sim 78^\circ\text{W}$ , and further decreases to a mean value of  $85 \pm 55\text{ cm}^{-3}$  over the remote region. The domain average near-surface  $N_d$  of  $154\text{ cm}^{-3}$  measured by the RB (Table 3) is in-between the mean  $N_d$  values of  $164\text{ cm}^{-3}$  and  $142\text{ cm}^{-3}$  based on aircraft and MODIS measurements during the VOCALS-REx obtained by Bretherton et al. (2010), in which their focus region was along  $20^\circ\text{S}$  and multiple aircraft measurements of  $N_d$  were included. The modeled cloud droplet concentrations are lower by 21 % and 13 % over the coastal and the remote regions, respectively, which is related to the low biases in the predicted aerosol concentrations.

### 3.2.2 Aerosol mass and composition

Aerosol mass and composition are other important measures and when combined with aerosol number, they can be used to derive aerosol information such as aerosol volume, surface area, and density. Over the SEP, the observed and simulated submicron aerosol mass is dominated by sulfate over both the coastal and remote regions for the measured chemical species (i.e., sulfate, nitrate, ammonium, organic carbon, chloride, and sodium). Observed and modeled MBL submicron aerosol mass concentrations of the different chemical species are shown in Fig. 4 and Table 4. Observations and the AERO both show that sulfate contributes to  $>55\%$  of the submicron aerosol mass among the four species measured by the AMS.

The predicted non-sea-salt sulfate concentrations over the coastal region are roughly 37 % and 15 % lower than the observed values, which are  $0.85\text{ }\mu\text{g m}^{-3}$  and  $1.13\text{ }\mu\text{g m}^{-3}$  based on the AMS instruments onboard the C-130 and RB, respectively. Observed sulfate concentrations over the remote region are  $\sim 0.30\text{--}0.40\text{ }\mu\text{g m}^{-3}$  (Table 4). These observed values over both coastal and remote regions are in general agreement

**Assessing regional  
scale predictions of  
marine  
stratocumulus**

Q. Yang et al.

[Title Page](#)[Abstract](#)[Introduction](#)[Conclusions](#)[References](#)[Tables](#)[Figures](#)[⏪](#)[⏩](#)[◀](#)[▶](#)[Back](#)[Close](#)[Full Screen / Esc](#)[Printer-friendly Version](#)[Interactive Discussion](#)

with Fig. 8 of Allen et al. (2011). The corresponding predicted values are, on average, 35–62 % lower. For the supermicron sulfate, observations show similar values ( $\sim 0.55 \mu\text{g m}^{-3}$ ) between remote and coastal regions. The simulated supermicron sulfate was close to observations (11 % lower) over the coastal region, but was 80 % lower over the remote region. The larger bias over the remote region suggests the underestimation of sulfate from DMS oxidation or too rapid sulfate removal, as addressed in more detail later in Sect. 4.

For ammonium mass concentrations, the simulated values are significantly smaller than the corresponding measurements for both the submicron ( $0.07\text{--}0.12 \mu\text{g m}^{-3}$  vs.  $0.10\text{--}0.30 \mu\text{g m}^{-3}$ ) and supermicron sizes ( $0.08 \mu\text{g m}^{-3}$  vs.  $0.23 \mu\text{g m}^{-3}$ ) over the coastal region (Table 4). Over the remote region, the detected ammonium ion concentrations (Table 4) are only slightly above instrument detection limits. The differences between values observed by the RB and that of the C-130 over this region reflect the difference in instrument detection limits. The corresponding predicted submicron ammonium is also small ( $<0.03 \mu\text{g m}^{-3}$ ) over the remote region. Both observations and the simulation indicate only trace amounts of nitrate.

The observed organic matter (OM) concentrations from different observation platforms are  $0.19\text{--}0.32 \mu\text{g m}^{-3}$  over the coastal region, which are underpredicted in the model by 25–56 %. Over the remote region, the C-130 and RB observed very different OM concentrations ( $0.08 \mu\text{g m}^{-3}$  vs.  $0.25 \mu\text{g m}^{-3}$ ), which are related to differences in sampling upper cutoff diameters and instrument detect limits. AERO does not include oceanic emissions of organic compounds, so the simulated  $\sim 0.03\text{--}0.04 \mu\text{g m}^{-3}$  OM over the remote region is solely due to continental sources. However, in clean maritime air masses, the contribution of OM from oceanic emissions to total organic mass could be significant (as much as 71 %) over the SEP region (Hawkins et al., 2010). Lower OM concentrations in MOSAIC could also result from not including secondary organic aerosol (SOA) processes. The contribution of SOA to OM is variable depending on factors such as precursor concentrations, oxidant level, etc., and the organic mass associated with clean marine air (Hawkins et al., 2010).

**Assessing regional  
scale predictions of  
marine  
stratocumulus**

Q. Yang et al.

Title Page

Abstract

Introduction

Conclusions

References

Tables

Figures

⏪

⏩

◀

▶

Back

Close

Full Screen / Esc

Printer-friendly Version

Interactive Discussion



The mean simulated chloride and sodium aerosol mass with diameters below  $1.5\ \mu\text{m}$  is in good agreement (21–35 % higher) with those sampled by the PILS ( $0.24\ \mu\text{g m}^{-3}$  for chloride and  $0.40\ \mu\text{g m}^{-3}$  for sodium) over the coastal region. The submicron chloride sampled on the RB has a domain-average of  $0.04\ \mu\text{g m}^{-3}$ , which is overpredicted by ~50 % in AERO (Table 4). The predicted supermicron chloride concentrations ( $6.25$ – $8.81\ \mu\text{g m}^{-3}$ ) are approximately twice the observed values ( $3.02$ – $4.18\ \mu\text{g m}^{-3}$ ) over the coastal and the remote regions (Table 4). The AERO predicted sodium concentrations are a factor of 2.0–2.4 higher than the RB observed values (Table 4). Note that treating sea salt as NaCl in the model implies an overestimation of the sodium and chloride emissions by 25 % and 10 %, respectively. After accounting for this effect, the supermicron sodium and chloride are overestimated by a factor of 1.9. The overestimation in the supermicron sizes could be related to errors in the predicted sea-salt size spectrum, which could also affect modeled dry deposition of larger particles.

As shown in Fig. 4, both observations and the simulation show 2–3 times higher total submicron mass concentration over the coastal region compared to the remote region. This highlights the importance of continental sources and the resulting outflow over maritime regions near the coast.

### 3.2.3 AOD

AOD is an important wavelength-dependent property that directly relates to aerosol direct radiative forcing, and is a function of the aerosol loading, composition, and size distribution. The AOD at  $0.55\ \mu\text{m}$  spectral wavelength from MODIS is compared with the coincident data from AERO in Fig. 5 for the VOCALS-REx period. The model reproduces the general spatial features observed by the satellite quite well. The domain-average AODs are  $0.10 \pm 0.06$  and  $0.11 \pm 0.06$  for MODIS and the AERO simulation, respectively. Both the model and observations show that high AOD values (i.e.,  $> 0.2$ ) are located along the coast, especially in a broad band with peak AOD values of approximately 0.3–0.4 off the northern Peruvian coast. The strong AOD gradient near the coast suggests influences from continental pollution outflow, which is also consistent

with the longitudinal variation of aerosols from in-situ instruments (Fig. 3). Along-shore winds associated with high-pressure systems combined with the Andes that form a physical barrier lead to aerosol transport from continental sources such as Santiago, Chile, to the northern coastal region (Huneess et al., 2006). Discrepancies between AERO and the observed AOD include a broader band of enhancements near the Peruvian coast and a lack of increased AOD values along the northern part of the western lateral boundary. The latter issue is most likely due to an under-estimation of oceanic emissions, or over-estimations of aerosol dry deposition and/or wet scavenging in this region. Both the model and observations have smaller AOD values farther offshore south of  $\sim 23^\circ$  S, where the dominant westerly surface flow often brings in relatively clean marine air (Bretherton et al., 2004).

### 3.3 Effective radius, cloud water path, and cloud optical thickness

Simulated cloud optical properties, which are cloud top effective radius ( $r_e$ ), cloud water path (CWP), and cloud optical thickness (COT), are compared against those from MODIS. As shown in Fig. 6 and Table 5, AERO results agree better with observations than do MET results for these three cloud properties.

MODIS  $r_e$  has a distinct longitudinal gradient north of  $30^\circ$  S (Fig. 6) with values increasing from  $\sim 8 \mu\text{m}$  right off the coast to  $> 16 \mu\text{m}$  near  $90^\circ$  W. This spatial distribution is consistent with the AOD gradient shown in Fig. 5, which is indicative of the first aerosol indirect effect. A similar longitudinal  $r_e$  gradient is simulated in AERO, though the large  $r_e$  south of  $30^\circ$  S is not well captured in the model. The domain-average  $r_e$  is  $13.4 \pm 2.6 \mu\text{m}$  for the satellite observations and  $11.9 \pm 1.8 \mu\text{m}$  for AERO. In comparison, MET substantially underestimated  $r_e$  ( $8.5 \pm 0.6 \mu\text{m}$ ), due to the use of the default, constant cloud droplet number concentration of  $250 \text{ cm}^{-3}$ , which is representative of the conditions near land (Fig. 3). The high and uniform droplet number concentration in MET not only causes the underestimation but also limits the variability of  $r_e$ .

## Assessing regional scale predictions of marine stratocumulus

Q. Yang et al.

Title Page

Abstract

Introduction

Conclusions

References

Tables

Figures



Back

Close

Full Screen / Esc

Printer-friendly Version

Interactive Discussion



**Assessing regional  
scale predictions of  
marine  
stratocumulus**

Q. Yang et al.

[Title Page](#)[Abstract](#)[Introduction](#)[Conclusions](#)[References](#)[Tables](#)[Figures](#)[⏪](#)[⏩](#)[◀](#)[▶](#)[Back](#)[Close](#)[Full Screen / Esc](#)[Printer-friendly Version](#)[Interactive Discussion](#)

The domain-average CWP is  $93 \pm 23 \text{ g m}^{-2}$  based on satellite retrievals, and it is underestimated (20%) and overestimated (23%), by AERO and MET, respectively. The mean CWP in AERO has excellent agreement (<5%) with observations over the coastal region, but is ~29% lower than observed values over the remote region. The low bias in AERO over the remote region might be related to low biases of moisture and droplet number. Low droplet number concentrations due to under-predicted aerosol concentrations result in shorter cloud lifetime. Larger CWP in MET is likely due to the high cloud droplet number ( $250 \text{ cm}^{-3}$ ) that substantially suppressed autoconversion and drizzle.

Both AERO and MET overestimate the COT but with a substantially high bias (~100%) seen in MET (Fig. 6 and Table 5). The doubled COT in MET is related to its near constant small  $r_e$  ( $10 \mu\text{m}$ ) and the overestimated CWP that are used in calculating COT (i.e.,  $\text{COT} \sim \text{cloud water content}/r_e$ ).

### 3.4 Cloud fraction, cloud base, and cloud thickness

Figure 7 shows mean low cloud fractions retrieved from GOES-10, and those in the AERO and MET during VOCALS-REx. The presence of low clouds is diagnosed based on the criterion of cloud water mixing ratio exceeding a threshold of  $0.01 \text{ g kg}^{-1}$  anywhere in a grid column below 700 hPa. The resulting cloud fraction for the column is then set to either 0 or 1. When averaging over the simulation period, the cloud fraction represents the frequency of cloud occurrence.

Satellite observations reveal more cloudiness during the night than during the day with a maximum located near  $20^\circ \text{ S}$  and several degrees in longitude away from the coastline. AERO and MET broadly reproduce the day-night contrast as well as the northeast-southwest gradients in cloudiness as seen in satellite observations. The domain-average low cloud fraction from satellite is  $75 \pm 8\%$  during the day and  $87 \pm 7\%$  during the night (Table 5), which are well predicted (< 3% biases) in both AERO and MET simulations with MET having slightly better agreement with observations. While

AERO mean cloud fractions are overestimated (3–4 %) over the coastal region, they are underestimated by 7 % over the remote region (i.e. near the south and west boundaries of the domain), as discussed in more detail in Sect. 4.

The near-coast minimum in low cloud fraction resulting from enhanced orographic subsidence associated with synoptic-scale ridging (Toniazzi et al., 2011) is evident in GOES-10 data with minimum values around 15° S and south of 20° S along the coastline during the day. The nighttime near-coast minimum cloudiness appears at similar locations as in the daytime along the northern Chile coastline but with higher values. Both AERO and MET are able to capture the minimum cloud fractions at these locations but to a smaller spatial extent. An exception is along the coast south of 23° S where the simulated cloud fraction exceeds 80 % at night. Between the two minima, both the observed and simulated results show high cloud fractions along the coastline which are likely associated with the dynamical blocking of the surface wind by the southern Peruvian Andes, leading to convergence and a mean upward motion (Garreaud and Munoz, 2005).

Both AERO and MET modeled cloud base and cloud thickness are in excellent agreement with the observations (Fig. 8 and Table 5), with better estimates seen in AERO (mean biases of <7 m for mean cloud base height and <1 m for mean cloud thickness). AERO does particularly well at simulating the frequency of clouds thicker than about 500 m, while MET overestimates these thicker clouds and underestimates clouds between 300 and 500 m thick.

### 3.5 TOA and surface energy fluxes

Top-of-the-atmosphere (TOA) and surface energy fluxes are modulated by water vapor, aerosol, and, most importantly, cloud properties such as cloud fraction and cloud optical depth. The simulated TOA outgoing SW fluxes are compared against those measured by CERES onboard the Terra satellite (Fig. 9).

The spatial pattern of satellite TOA outgoing SW fluxes is consistent with the broad feature of the observed daytime cloud fraction shown in Fig. 7. The observed SW fluxes

## Assessing regional scale predictions of marine stratocumulus

Q. Yang et al.

Title Page

Abstract

Introduction

Conclusions

References

Tables

Figures



Back

Close

Full Screen / Esc

Printer-friendly Version

Interactive Discussion



have a band of maximum values ( $>450 \text{ W m}^{-2}$ ) nearly parallel to the Peruvian coastline. As shown in Table 6, the domain-average SW flux simulated by AERO ( $348 \text{ W m}^{-2}$ ) is identical to the satellite retrievals, although this is due to compensation between high and low biases ( $\sim 10\%$ ) over the coastal and the remote regions, respectively. AERO has a band of maximum fluxes roughly collocated with the observed maximum. But the observed SW minimum along the coast near  $15^\circ \text{ S}$  is not well captured. For this particular region, although AERO simulated COT is smaller than observations (Fig. 6), the impact of this low bias on outgoing SW fluxes is compensated by overestimations of both AOD and cloud fraction (Fig. 7). In AERO, the biases in cloud fraction correlate well with the biases in TOA SW, for example, the low biases near the west boundary correspond to the underestimation of cloudiness in this region. In the MET simulation, TOA SW fluxes are overestimated by  $\sim 10\%$  over both coastal and remote regions. In addition to the positive bias in the predicted cloud fraction near the coast, the substantial overprediction of cloud optical thickness in MET (Fig. 7) also contributes to the high bias.

The TOA satellite comparison presents a regional view. Alternatively, a sonic anemometer onboard the RB monitored surface fluxes at a high time frequency along the ship track allowing us to examine the associated longitudinal and diurnal variations (Fig. 10). The observed surface fluxes include sensible heat, latent heat, downward shortwave, and downward longwave fluxes (Table 6). Observed sensible heat fluxes are small ( $4 \text{ W m}^{-2}$ ) with a weak longitudinal gradient. The sensible heat fluxes from AERO and MET are biased high with means of  $12 \text{ W m}^{-2}$  and  $9 \text{ W m}^{-2}$ , respectively, and have a more distinct increasing trend towards the west. Associated with solar heating of the atmosphere, both observed and simulated sensible heat fluxes have a decreasing tendency from late morning to the afternoon (10:00–17:00 local time), although this decreasing tendency continues to late evening (22:00 local time) in the observations but ends several hours earlier in the simulations.

Both measured and modeled surface latent heat fluxes increase with distance from the coast due to the increasing SST. Simulated dry biases in the MBL over the remote

## Assessing regional scale predictions of marine stratocumulus

Q. Yang et al.

[Title Page](#)[Abstract](#)[Introduction](#)[Conclusions](#)[References](#)[Tables](#)[Figures](#)[⏪](#)[⏩](#)[◀](#)[▶](#)[Back](#)[Close](#)[Full Screen / Esc](#)[Printer-friendly Version](#)[Interactive Discussion](#)

region lead to the overestimation of the latent heat fluxes over this region. The observed surface latent heat flux has a mean value of  $91 \text{ W m}^{-2}$ . The mean latent heat flux from AERO ( $100 \text{ W m}^{-2}$ ) shows a slight improvement from that ( $103 \text{ W m}^{-2}$ ) of MET. The observed latent heat fluxes do not have a distinct diurnal variation; the simulated latent heat has biases which peak in the early morning.

The mean SW flux from observations and AERO agree within 2% over the coastal region, and is  $\sim 8\%$  lower over the remote region. The MET simulation underestimates SW fluxes by  $\sim 15\%$  over the coastal region, but overpredicts by 5% over the remote region. The apparent better-predicted SW fluxes over the coastal region in AERO compared to MET indicate better-predicted daytime cloud covers along the path of the ship in AERO over this region. The diurnal variation of incoming SW fluxes shown in Fig. 10 is plotted as differences between modeled and observed values due to the large diurnal cycle. Both simulations tend to underpredict SW in the morning; AERO shows apparent better predictions than does MET in the afternoon. The analysis shown here is a direct comparison of measured and observed data in corresponding times and locations and does not account for the large instant biases in SW due to prediction biases in instantaneous cloud fields. Therefore, given this strict comparison, the results are quite good.

Predicted downward longwave fluxes and observations are in good agreement with mean differences of less than  $1 \text{ W m}^{-2}$ . The observed downward longwave fluxes have a distinct diurnal variation with higher values ( $\sim 380 \text{ W m}^{-2}$ ) at night and a minimum ( $\sim 350 \text{ W m}^{-2}$ ) in the afternoon (15:00 local time). The AERO simulates a slightly better variation than does the MET during the day. The diurnal and longitudinal variations of the surface downwelling SW and LW fluxes are likely caused by corresponding variations in clouds.

## Assessing regional scale predictions of marine stratocumulus

Q. Yang et al.

[Title Page](#)[Abstract](#)[Introduction](#)[Conclusions](#)[References](#)[Tables](#)[Figures](#)[⏪](#)[⏩](#)[◀](#)[▶](#)[Back](#)[Close](#)[Full Screen / Esc](#)[Printer-friendly Version](#)[Interactive Discussion](#)

### 3.6 Rain rate

Rain rate in marine stratocumulus is tightly connected to both cloud macro and micro-physical properties, and rain processes exert important feedbacks to the MBL through redistribution of heat and moisture. Modeled rain rates are compared against those derived from measurements by a 2D-C probe onboard the C-130 aircraft. Mean and median in-cloud and near surface rain rate values are presented in Table 7. In-cloud rain rates are averaged over the in-cloud flight legs with various depths in the cloud layer, and “in-cloud” is determined from flight elevations and the radar/lidar retrievals of cloud height information.

Noticeable longitudinal gradients exist in observed in-cloud and near-surface rain rates ( $\sim 200$  m above the ocean surface). Observed average in-cloud rain rates increase by about 10-fold ( $0.668$  vs.  $6.891$   $\text{mm day}^{-1}$ ) from the coastal to the remote region (Table 7). Overall, the longitudinal variations in rain rates are captured in model simulations but predicted rain rates are about an order of magnitude smaller than the observed values within the cloud layer (Fig. 11 and Table 7). AERO produces higher rain rates than the MET, with the AERO median rain rates generally close to the 75th percentile of MET, resulting in closer agreement with observations for AERO.

In the near-surface layer, drizzle was barely observed over the coastal region. Over the remote region although the observed mean near-surface rain rate is  $\sim 75\%$  of the in-cloud value, the median rain rate in near-surface layer is drastically smaller than the in-cloud value ( $0.002$  vs.  $0.396$   $\text{mm day}^{-1}$ ). The observed strong near-surface/in-cloud contrast seen in median rain rates but not in the means could be explained by the skewed distribution of rain rates. Light rain occurs more frequently in the SEP stratocumulus, dominates the median value, and is associated with smaller mean raindrop size and relatively high evaporation rates below clouds. In contrast, the mean precipitation rate is dominated by relatively heavier rain, which is associated with larger mean raindrop size and hence relatively lower evaporation rates below clouds. In both simulations, the near-surface/in-cloud rain rate contrasts are not well represented, although

## Assessing regional scale predictions of marine stratocumulus

Q. Yang et al.

Title Page

Abstract

Introduction

Conclusions

References

Tables

Figures

⏪

⏩

◀

▶

Back

Close

Full Screen / Esc

Printer-friendly Version

Interactive Discussion



these observed contrasts might be larger than in reality due to a 62.5  $\mu\text{m}$  lower rain-drop cutoff diameter in measurements. Evaporation below cloud base might shrink raindrops to sizes smaller than 62.5  $\mu\text{m}$  at the near-surface layer, which could not be detected by the 2D-C probe.

In addition, the model did not reproduce the large variability in observed rain rates. The observed rain rates are as high as 100  $\text{mm day}^{-1}$  on some flight legs, as indicated by the outliers (red circles in Fig. 11), yet the modeled drizzle rates barely exceed 2  $\text{mm day}^{-1}$ . This is most likely a model resolution issue. The rain rates derived from flight data were averaged over about 9-km flight distance, which is comparable to our model horizontal grid size. However, the WRF model is known to actually resolve processes at scales about 7 times of the horizontal grid spacing (Skamarock, 2004). Higher vertical and horizontal resolution simulations will be conducted in a follow-on study to explore this resolution issue.

## 4 Discussion

In this section, we elaborate on a few points related to model-observation comparisons described previously.

Observations show that the MBL is more well-mixed, colder and less humid over the coastal region (70–78° W) than over the remote region (78–88° W). The simulated mean MBL temperature and humidity, in general, are in good agreement with the observed values over the coastal region, but larger biases are found over the remote region with  $\sim 2\text{ K}$  cold bias and  $\sim 1\text{ g kg}^{-1}$  low bias in humidity in both AERO and MET simulations. These low biases impact the predictions of cloud fraction, SW, sensible heat, and latent heat over the remote region. The observed large variability of the moisture and temperature profiles over the remote ocean is not well represented in both simulations. This might be related to the lack of representation of open to closed cellular dynamics in the model which impacts more of the remote region where clouds are characterized by the open cellular structure.

### Assessing regional scale predictions of marine stratocumulus

Q. Yang et al.

Title Page

Abstract

Introduction

Conclusions

References

Tables

Figures



Back

Close

Full Screen / Esc

Printer-friendly Version

Interactive Discussion



**Assessing regional  
scale predictions of  
marine  
stratocumulus**

Q. Yang et al.

Title Page

Abstract

Introduction

Conclusions

References

Tables

Figures



Back

Close

Full Screen / Esc

Printer-friendly Version

Interactive Discussion



The predicted MBL depth has a 150-m reduction when aerosol-cloud interactions are included in the model simulation (i.e., in AERO). Processes at different scales influence MBL depths over the SEP. For example, large-scale subsidence tends to suppress the growth of MBL; horizontal advection may affect tendencies of MBL depth when its gradients exist along wind directions (Rahn and Garreaud, 2010); active turbulence mixing corresponds to higher MBL, and entrainment deepens and dries the MBL (Wood and Bretherton, 2004; Zuidema et al., 2009). Lower MBL depths in AERO compared to MET indicate the active role of aerosol and aerosol-cloud interactions in modifying those MBL processes. The AERO, compared to MET, also produces improved moisture and temperature gradients in the capping inversion layer. The strengthening of the inversion near the coast by including aerosol in the model is likely due to the atmospheric diabatic heating induced by direct effect of the absorbing aerosols and the resulting semi-direct effect of enhancing cloud evaporation (Matsui et al., 2006; Dunion and Velden, 2004). Particularly, compared to the MET, the stronger inversion in the AERO leads to weaker entrainment and limits the vertical growth of the MBL.

Followed by MBL structures, simulated MBL aerosol is evaluated against observations in number, mass composition, and optical properties. The observed strong gradient in accumulation mode (0.16–2.69  $\mu\text{m}$ ) aerosol number concentrations near the coast over the SEP region are also predicted reasonably well in the AERO simulation. The predicted aerosol number has a low bias of about  $\sim 30\%$ , which is in rather good agreement for simulating aerosol number. The longitudinal variation in droplet number, in general, corresponds to the spatial variation in aerosols. Consistent with the underestimation of accumulation mode aerosol, the in-cloud droplet number concentrations are also too low.

Non-sea-salt sulfate is the dominant aerosol species in submicron mass concentration over both coastal and remote regions within SEP MBL. It is tempting to attribute the larger underprediction in sulfate mass over the remote region compared to the coastal region (35–62 % vs. 11–37 %) to the underprediction of secondary sulfate produced from DMS oxidation. However, further investigation does not support this

## Assessing regional scale predictions of marine stratocumulus

Q. Yang et al.

Title Page

Abstract

Introduction

Conclusions

References

Tables

Figures

⏪

⏩

◀

▶

Back

Close

Full Screen / Esc

Printer-friendly Version

Interactive Discussion

explanation. The mean AERO-predicted DMS air mixing ratio is approximately a factor of 3 higher than the mean RB observations (Table 3) which can be partially explained by the  $\sim 71\%$  overestimation of the DMS ocean-to-atmosphere transfer velocity ( $K_w$ ). The high bias in  $K_w$  occurs mainly at higher wind speeds (not shown), consistent with Yang et al. (2009). Another source of error is the setting of a constant oceanic DMS as required by the VOCA model intercomparison specifications. However, given the transfer velocity overestimate, the prescribed sea-water DMS would have to be unrealistically low to cause the sulfate bias. Despite the high predicted DMS levels relative to observations, predicted MBL  $\text{SO}_2$  mixing ratios are underestimated (8.6 vs. 35.5 pptv) over the remote region. Sensitivity tests show that most of the emitted DMS converts to  $\text{SO}_2$ , which then converts to sulfate primarily via aqueous phase cloud chemistry reactions. Speeding up the DMS gas-phase chemistry lowers DMS air concentrations but has little impact on sulfate (not shown). Therefore, the underestimation of sulfate is unlikely due to modeled DMS emissions or oxidation. An alternate explanation is that wet removal of sulfate, particularly that just formed by cloud chemistry, is too rapid in the model, and this needs further investigation. The underestimation of sulfate near the coast is likely due to errors in continental emissions and/or transport biases.

The simulated chloride and sodium concentrations for diameters below  $1.5\ \mu\text{m}$  are in good agreement with observations, but the supermicron concentrations are approximately double the observations. This suggests possible errors in the predicted sea-salt size spectrum for larger sizes ( $>1.5\ \mu\text{m}$ ), which could also affect the modeled dry deposition. More detailed observed sea-salt size distributions are not available; however, the substantial overestimation in the mass demonstrates the need to further evaluate the sea-salt emission scheme used in WRF-Chem to bring mass concentrations and sizes of sea-salt particles to better agreement with the observations.

Anthropogenic outflow and synoptic influences to the spatial variation of the mean AOD field are apparent in both satellite observations and simulations. Simulated AOD values agree well with observations on a domain-average basis, although the near-coast enhancements cover a broader area in the model. The high AOD close to the

coast is consistent with the predicted aerosol mass along the G-1 flight tracks that was also somewhat higher than observed (Fig. 4).

Despite the inevitable uncertainties in predicting aerosol mass, composition, and size distribution, cloud optical properties are, in general, better simulated in the AERO than in the MET. In the simulations, the location of high aerosol loading mostly corresponds to low CWP over the coast. Higher cloud droplet numbers at a polluted environment are associated with a more stable atmosphere (Painemal and Zuidema, 2010; and references therein), and model simulations by Jiang et al. (2002) found that simulated stable atmosphere due to drizzle inhibition further reduces the moisture supply and leads to low CWP (Matsui et al., 2006).

Inclusion of interactive aerosols in AERO also lead to better simulated cloud top optical properties ( $r_e$ , CWP, and COT).

Predicted period-mean cloud fields from both simulations are in good agreement with the satellite observations. While AERO slightly overestimates (3–4 %) over the coastal region, cloud fractions are underestimated by ~7 % over the remote areas which is mainly due to the underestimation of cloudiness close to the west and south boundaries of the model domain. The underprediction of cloud fraction over the west and south boundaries also results in a negative bias in TOA SW compared to satellite observations. In AERO, the low humidity bias over the remote area might contribute to the low cloud fraction over this region. In addition, small cloud droplet number concentrations near west and south boundaries allow droplets to grow into large raindrops which deplete the available liquid water leading to underestimation in cloud fraction in these areas. In MET, the low MBL humidity bias over the remote region might be compensated by the large droplet number concentration, leading to a several percent higher mean cloud fraction than the AERO simulation. The predicted cloud base and cloud thickness are in excellent agreement with the observations in AERO. This better prediction compared to MET is consistent with the better-predicted MBL structure and better-simulated CWP variations in AERO.

**Assessing regional scale predictions of marine stratocumulus**

Q. Yang et al.

Title Page

Abstract

Introduction

Conclusions

References

Tables

Figures



Back

Close

Full Screen / Esc

Printer-friendly Version

Interactive Discussion



## Assessing regional scale predictions of marine stratocumulus

Q. Yang et al.

Title Page

Abstract

Introduction

Conclusions

References

Tables

Figures

⏪

⏩

◀

▶

Back

Close

Full Screen / Esc

Printer-friendly Version

Interactive Discussion



Both AERO and MET show near-coast cloud fraction minima over similar locations as observed but to a smaller spatial extent, with the exception along the coast south of about 23° S where the simulated cloud fraction exceeds 80 % at night. Fairly simulated near-coast clear skies in MET indicates that the near-coast clearness is a largely synoptic induced event as concluded by Toniazzo et al. (2011) and references therein.

The TOA outgoing SW fluxes manifest the cloud albedo effect, and are closely related to cloud fraction and cloud top  $r_e$ . The domain-average SW flux simulated in AERO is similar to the observed ( $347 \pm 59 \text{ W m}^{-2}$ ), although this is the result of a high bias ( $49 \text{ W m}^{-2}$ ) over the coastal region and a low bias ( $23 \text{ W m}^{-2}$ ) over the remote region. The positive bias in TOA SW over the coastal region in AERO is related to the overprediction of the near-coast cloud fraction. The negative biases near the west boundary in the AERO are related to the aforementioned underestimation of cloud fraction near west and south boundaries. MET overestimates TOA SW by  $35 \text{ W m}^{-2}$  over both coastal and remote regions. In MET, the overprediction of cloud optical thickness in the SW scheme also contributes to the high bias in mean cloud albedo.

Sensible heat fluxes are small but they are significantly overestimated in both simulations over the remote region. The SST and 10-m wind speed in the simulations are in close agreement with observations (Table 3), therefore, the positive bias in sensible heat over the remote region is associated with the predicted negative bias ( $-2 \text{ K}$ ) in MBL temperature over this region. The overpredicted surface latent heat fluxes (by  $\sim 20\%$  in AERO and by  $\sim 30\%$  in MET) correspond to the negative biases ( $-1 \text{ g kg}^{-1}$ ) in humidity. Surface incoming longwave fluxes have better agreement with observations over the coastal region and in the overall diurnal cycles in AERO. Downwelling SW fluxes are better predicted over the coast region and in the afternoon in AERO.

The simulated in-cloud drizzle rates have similar longitudinal gradients as seen in the observations, although they are significantly underestimated and have low variability. Without a shallow convection scheme, the model will not be able to reproduce the observed heavier rains such as those  $>100 \text{ mm day}^{-1}$ . Even with a shallow convection scheme, the model will probably not be able to produce correct heat

and moisture transports that are crucial in sustaining the organized precipitating stratocumulus clouds, since the PBL parameterization is not designed to handle open-cell dynamics. In addition, our 9-km horizontal spacing is inadequate in resolving open cellular cloud structures, although the vertical model resolution of 50 m is comparable to the 30 m used in the large-eddy simulation (LES) in Wang and Feingold (2009a, b). Observations (e.g., Wood et al., 2011a) and LES simulations (e.g. Wang and Feingold, 2009a, b) found that strongly precipitating stratocumulus clouds typically consist of narrow open-cell walls of less than 10 km in width which is much smaller than our model's effective resolution ( $\sim 7\Delta x$ ). Therefore, horizontal resolutions as well as simulated temperature and humidity biases/variability are likely to be responsible for the inability of our simulations to reproduce correct precipitation variability. Future studies will be conducted to investigate this resolution-related issue with an ultimate goal of improving the parameterization of stratocumulus-related sub-grid scale processes in climate models.

## 5 Summary and conclusion

In this study, we tested the new coupling between the Morrison double-moment microphysics scheme and interactive aerosols in WRF-Chem. This modeling capability has been frequently requested by the WRF community, and it is anticipated that the community will use it extensively. The WRF-Chem 31-day (15 October–16 November 2008) simulation with aerosol-cloud interactions is compared to a simulation with fixed cloud droplet number concentrations assumed by the default in Morrison microphysics scheme with no interactive aerosols. The extensive measurements collected during VOCALS-REx were used to evaluate predicted aerosols, marine stratocumulus clouds, and their interactions. The well-predicted aerosol quantities such as aerosol number, mass composition and optical properties lead to significant improvements in many features of the predicted stratocumulus clouds: cloud optical properties and microphysical properties such as cloud top effective radius, cloud water path, and cloud optical thickness, and cloud macrostructure such as cloud depth and cloud base height.

### Assessing regional scale predictions of marine stratocumulus

Q. Yang et al.

Title Page

Abstract

Introduction

Conclusions

References

Tables

Figures



Back

Close

Full Screen / Esc

Printer-friendly Version

Interactive Discussion



---

**Assessing regional  
scale predictions of  
marine  
stratocumulus**Q. Yang et al.

---

[Title Page](#)[Abstract](#)[Introduction](#)[Conclusions](#)[References](#)[Tables](#)[Figures](#)[Back](#)[Close](#)[Full Screen / Esc](#)[Printer-friendly Version](#)[Interactive Discussion](#)

In addition to accounting for the aerosol direct and semi-direct effects, these improvements feed back to the prediction of boundary-layer characteristics and energy budgets. Particularly, inclusion of interactive aerosols in AERO strengthens the temperature and humidity gradients within the capping inversion layer and lowers the marine boundary layer depth by 150 m from that of the MET simulation. Mean TOA outgoing shortwave fluxes, surface latent heat, and surface downwelling longwave fluxes are in better agreement with observations in AERO, compared to the MET simulation.

Nevertheless, errors in some of the simulated meteorological and aerosol quantities likely affect simulated stratocumulus and energy fluxes over the SEP. For example, temperature and humidity low biases in the remote MBL are linked to the underpredictions in TOA SW, cloud fraction, and rain rates as well as overpredictions in surface sensible heat and latent heat fluxes.

The simulations conducted as part of this study were submitted to the VOCALS modeling assessment that will be published in the near future. This paper supplements the upcoming broad assessment by showing links between aerosols and clouds, and providing additional insights into the capability of current regional model with interactive aerosols in predicting aerosol and cloud fields over the SEP region. Our findings as presented in this paper will help explain some of the differences among model results in the assessment. Our evaluation also implies the importance of aerosol-cloud interactions in climate modeling. Results from this study illustrate that an accurate representation of aerosol properties, variations, and their interactions with clouds in models could improve the MBL structure, TOA/surface energy fluxes, and cloud properties in regional scale simulations; similar improvements are expected in climate models with aerosol-cloud interactions. This study compared two extreme cases: one with prognostic aerosol and the other with a cloud droplet concentration that is fixed in space and time. It might be possible to reasonably capture the spatial and temporal variability of the microphysics using prescribed temporal/spatial gradients of droplet concentrations or background aerosol.

## Assessing regional scale predictions of marine stratocumulus

Q. Yang et al.

Title Page

Abstract

Introduction

Conclusions

References

Tables

Figures

⏪

⏩

◀

▶

Back

Close

Full Screen / Esc

Printer-friendly Version

Interactive Discussion



Although not perfect, the overall performance of the model in simulating mesoscale aerosol-cloud interactions associated with marine stratocumulus is encouraging. This study focused on MBL characteristics rather than large-scale dynamics, and additional research is needed to investigate the impacts of parameterized mixing, entrainment, and large-scale dynamics on the simulated aerosol, clouds, and precipitation. This study is the necessary first step to form the foundation for a planned range of future studies using a similar model configuration. Simulations at smaller horizontal grid spacings will be presented in a follow-up study regarding the sensitivity of predicted aerosols, clouds, and their interactions to spatial resolution. In addition, multiple aerosol-cloud equilibrium regimes (Baker and Charlson, 1990) over the southeastern Pacific Ocean will be investigated using WRF-Chem in the near future.

*Acknowledgements.* The authors thank Elaine Chapman for her detailed comments and assistance with emissions for this paper. RB and C-130 measurements were obtained from the VOCALS data archive of NCAR/EOL, which is sponsored by the National Science Foundation. We also acknowledge Y.-N. Lee of Brookhaven National Laboratory for aerosol mass composition data, D. Leon and the staff of University of Wyoming for the Radar/Lidar derived cloud top and cloud base data, S. Abel and A. Grant for the low cloud fraction data retrieved from GEOS-10, C. Fairall and L. Bariteau for surface flux data, B. J. Huebert for DMS data, A. Schanot and J. Jensen for C-130 2D-C probe data and guidance in data usage, S. d. Szoeke, S. Yuter, and C. Fairall for Rawinsonde data, T. Bate for the aerosol composition data on the RB and guidance in data usage, S. Howell and L. Shank for the aerosol composition data on C-130, B. Alan for gas phase SO<sub>2</sub> measurements, etc. We also thank the many scientists who participated to generate VOCALS field campaign data set. MODIS and CERES data were obtained from the NASA Langley Research Center Atmospheric Science Data Center. Some of the analyses were completed using the Aerosol Modeling Testbed tools developed as part of the Aerosol Climate Initiative supported by Laboratory Directed Research Development program at Pacific Northwest National Laboratory. Funding for this research has been provided by the US NOAA Atmospheric Composition and Climate Program (NA10AANRG0083/56091).

## References

- Abel, S. J., Walters, D. N., and Allen, G.: Evaluation of stratocumulus cloud prediction in the Met Office forecast model during VOCALS-REx, *Atmos. Chem. Phys.*, 10, 10541–10559, doi:10.5194/acp-10-10541-2010, 2010.
- 5 Albrecht, B. A.: Aerosols, Cloud Microphysics, and Fractional Cloudiness, *Science*, 245, 1227–1230, 1989.
- Allen, G., Coe, H., Clarke, A., Bretherton, C., Wood, R., Abel, S. J., Barrett, P., Brown, P., George, R., Freitag, S., McNaughton, C., Howell, S., Shank, L., Kapustin, V., Brekhovskikh, V., Kleinman, L., Lee, Y.-N., Springston, S., Toniazzo, T., Krejci, R., Fochesatto, J., Shaw, G., Krecl, P., Brooks, B., McMeeking, G., Bower, K. N., I. Williams, P., Crosier, J., Crawford, I., Connolly, P., Allan, J. D., Covert, D., A. R. Bandy, Russell, L. M., Trembath, J., Bart, M., McQuaid, J. B., Wang, J., and Chand, D.: South East Pacific atmospheric composition and variability sampled along 20S during VOCALS-REx, *Atmos. Chem. Phys.*, 11, 5237–5262, doi:10.5194/acp-11-5237-2011, 2011.
- 15 Baker, M. B. and Charlson, R. J.: Bistability of CCN Concentrations and Thermodynamics in the Cloud-topped Boundary-Layer, *Nature*, 345, 142–145, 1990.
- Bretherton, C. S., Wood, R., George, R. C., Leon, D., Allen, G., and Zheng, X.: Southeast Pacific stratocumulus clouds, precipitation and boundary layer structure sampled along 20 degrees S during VOCALS-REx, *Atmos. Chem. Phys.*, 10, 10639–10654, doi:10.5194/acp-10-10639-2010, 2010.
- 20 Chapman, E. G., Gustafson Jr., W. I., Easter, R. C., Barnard, J. C., Ghan, S. J., Pekour, M. S., and Fast, J. D.: Coupling aerosol-cloud-radiative processes in the WRF-Chem model: Investigating the radiative impact of elevated point sources, *Atmos. Chem. Phys.*, 9, 945–964, doi:10.5194/acp-9-945-2009, 2009.
- 25 Clarke, A. D., Owens, S. R., and Zhou, J. C.: An ultrafine sea-salt flux from breaking waves: Implications for cloud condensation nuclei in the remote marine atmosphere, *J. Geophys. Res.-Atmos.*, 111, D06202, doi:10.1029/2005jd006565, 2006.
- DeCarlo, P. F., Kimmel, J. R., Trimborn, A., Northway, M. J., Jayne, J. T., Aiken, A. C., Gonin, M., Fuhrer, K., Horvath, T., Docherty, K. S., Worsnop, D. R., and Jimenez, J. L.: Field-deployable, high-resolution, time-of-flight aerosol mass spectrometer, *Anal. Chem.*, 78, 8281–8289, doi:10.1021/ac061249n, 2006.
- 30 Dunion, J. P. and Velden, C. S.: The impact of the Saharan air layer on Atlantic tropical cyclone

### Assessing regional scale predictions of marine stratocumulus

Q. Yang et al.

Title Page

Abstract

Introduction

Conclusions

References

Tables

Figures



Back

Close

Full Screen / Esc

Printer-friendly Version

Interactive Discussion



## Assessing regional scale predictions of marine stratocumulus

Q. Yang et al.

Title Page

Abstract

Introduction

Conclusions

References

Tables

Figures

⏪

⏩

◀

▶

Back

Close

Full Screen / Esc

Printer-friendly Version

Interactive Discussion



activity, *B. Am. Meteorol. Soc.*, 85, 353, doi:10.1175/BAMS-85-3-353, 2004.

Fast, J., Aiken, A. C., Allan, J., Alexander, L., Campos, T., Canagaratna, M. R., Chapman, E., DeCarlo, P. F., de Foy, B., Gaffney, J., de Gouw, J., Doran, J. C., Emmons, L., Hodzic, A., Herndon, S. C., Huey, G., Jayne, J. T., Jimenez, J. L., Kleinman, L., Kuster, W., Marley, N., Russell, L., Ochoa, C., Onasch, T. B., Pekour, M., Song, C., Ulbrich, I. M., Warneke, C., Welsh-Bon, D., Wiedinmyer, C., Worsnop, D. R., Yu, X.-Y., and Zaveri, R.: Evaluating simulated primary anthropogenic and biomass burning organic aerosols during MILAGRO: implications for assessing treatments of secondary organic aerosols, *Atmos. Chem. Phys.*, 9, 6191–6215, doi:10.5194/acp-9-6191-2009, 2009.

Fast, J. D., Gustafson, W. I., Easter, R. C., Zaveri, R. A., Barnard, J. C., Chapman, E. G., Grell, G. A., and Peckham, S. E.: Evolution of ozone, particulates, and aerosol direct radiative forcing in the vicinity of Houston using a fully coupled meteorology-chemistry-aerosol model, *J. Geophys. Res.-Atmos.*, 111, D21305, doi:10.1029/2005jd006721, 2006.

Garreaud, R. D. and Munoz, R. C.: The low-level jet off the west coast of subtropical South America: Structure and variability, *Mon. Weather Rev.*, 133, 2246–2261, 2005.

Gong, S. L., Barrie, L. A., and Blanchet, J. P.: Modeling sea-salt aerosols in the atmosphere .1. Model development, *J. Geophys. Res.-Atmos.*, 102, 3805–3818, 1997.

Grell, G. A., Peckham, S. E., Schmitz, R., McKeen, S. A., Frost, G., Skamarock, W. C., and Eder, B.: Fully coupled “online” chemistry within the WRF model, *Atmos. Environ.*, 39, 6957–6975, doi:10.1016/j.atmosenv.2005.04.027, 2005.

Guenther, A., Karl, T., Harley, P., Wiedinmyer, C., Palmer, P. I., and Geron, C.: Estimates of global terrestrial isoprene emissions using MEGAN (Model of Emissions of Gases and Aerosols from Nature), *Atmos. Chem. Phys.*, 6, 3181–3210, doi:10.5194/acp-6-3181-2006, 2006.

Gustafson, W. I., Chapman, E. G., Ghan, S. J., Easter, R. C., and Fast, J. D.: Impact on modeled cloud characteristics due to simplified treatment of uniform cloud condensation nuclei during NEAQS 2004, *Geophys. Res. Lett.*, 34, L19809, doi:10.1029/2007gl030021, 2007.

Hawkins, L. N., Russell, L. M., Covert, D. S., Quinn, P. K., and Bates, T. S.: Carboxylic acids, sulfates, and organosulfates in processed continental organic aerosol over the south-east Pacific Ocean during VOCALS-REx 2008, *J. Geophys. Res.-Atmos.*, 115, D13201, doi:10.1029/2009jd013276, 2010.

Hong, S. Y., Noh, Y., and Dudhia, J.: A new vertical diffusion package with an explicit treatment of entrainment processes, *Mon. Weather Rev.*, 134, 2318–2341, 2006.

## Assessing regional scale predictions of marine stratocumulus

Q. Yang et al.

Title Page

Abstract

Introduction

Conclusions

References

Tables

Figures

⏪

⏩

◀

▶

Back

Close

Full Screen / Esc

Printer-friendly Version

Interactive Discussion



Huneeus, N., Gallardo, L., and Rutllant, J. A.: Offshore transport episodes of anthropogenic sulfur in northern Chile: Potential impact on the stratocumulus cloud deck, *Geophys. Res. Lett.*, 33, L19819, doi:10.1029/2006gl026921, 2006.

Kleinman, L. I., Daum, P. H., Lee, Y.-N., Lewis, E. R., Sedlacek III, A. J., Senum, G. I., Springston, S. R., Wang, J., Hubbe, J., Jayne, J., Min, Q., Yum, S. S., and Allen, G.: Aerosol concentration and size distribution measured below, in, and above cloud from the DOE G-1 during VOCALS-REx, *Atmos. Chem. Phys. Discuss.*, 11, 17289–17336, doi:10.5194/acpd-11-17289-2011, 2011.

Loeb, N. G., Kato, S., Loukachine, K., and Manalo-Smith, N.: Angular distribution models for top-of-atmosphere radiative flux estimation from the Clouds and the Earth's Radiant Energy System instrument on the Terra satellite. Part I: Methodology, *J. Atmos. Ocean Tech.*, 22, 338–351, 2005.

Matsui, T., Masunaga, H., Kreidenweis, S. M., Pielke, R. A., Tao, W. K., Chin, M., and Kaufman, Y. J.: Satellite-based assessment of marine low cloud variability associated with aerosol, atmospheric stability, and the diurnal cycle (111, D17204, 2006), *J. Geophys. Res.-Atmos.*, 111, D20202, doi:10.1029/2006jd008056, 2006.

Monahan, E. C., Spiel, D. E., and Davidson, K. L.: A model of marine aerosol generation via whitecaps and wave disruption, in: *Oceanic Whitecaps*, edited by: Niocail, E. C. M. a. G. M., D. Reidel, Norwell, 167–174, 1986.

Morrison, H. and Pinto, J. O.: Mesoscale modeling of springtime Arctic mixed-phase stratiform clouds using a new two-moment bulk microphysics scheme, *J. Atmos. Sci.*, 62, 3683–3704, 2005.

Morrison, H., Pinto, J. O., Curry, J. A., and McFarquhar, G. M.: Sensitivity of modeled arctic mixed-phase stratocumulus to cloud condensation and ice nuclei over regionally varying surface conditions, *J. Geophys. Res.-Atmos.*, 113, D05203, doi:10.1029/2007jd008729, 2008.

Morrison, H., Thompson, G., and Tatarskii, V.: Impact of Cloud Microphysics on the Development of Trailing Stratiform Precipitation in a Simulated Squall Line: Comparison of One- and Two-Moment Schemes, *Mon. Weather Rev.*, 137, 991–1007, doi:10.1175/2008mwr2556.1, 2009.

Nightingale, P. D., Malin, G., Law, C. S., Watson, A. J., Liss, P. S., Liddicoat, M. I., Boutin, J., and Upstill-Goddard, R. C.: In situ evaluation of air-sea gas exchange parameterizations using novel conservative and volatile tracers, *Global Biogeochem. Cy.*, 14, 373–387, 2000.

Painemal, D. and Zuidema, P.: Microphysical variability in southeast Pacific Stratocumulus

## Assessing regional scale predictions of marine stratocumulus

Q. Yang et al.

Title Page

Abstract

Introduction

Conclusions

References

Tables

Figures

⏪

⏩

◀

▶

Back

Close

Full Screen / Esc

Printer-friendly Version

Interactive Discussion

clouds: synoptic conditions and radiative response, *Atmos. Chem. Phys.*, 10, 6255–6269, doi:10.5194/acp-10-6255-2010, 2010.

Qian, Y., Gustafson, W. I., Leung, L. R., and Ghan, S. J.: Effects of soot-induced snow albedo change on snowpack and hydrological cycle in western United States based on Weather Research and Forecasting chemistry and regional climate simulations, *J. Geophys. Res.-Atmos.*, 114, D03108, doi:10.1029/2008jd011039, 2009.

Rahn, D. A. and Garreaud, R.: Marine boundary layer over the subtropical southeast Pacific during VOCALS-REx – Part 1: Mean structure and diurnal cycle, *Atmos. Chem. Phys.*, 10, 4491–4506, doi:10.5194/acp-10-4491-2010, 2010.

Remer, L. A., Kleidman, R. G., Levy, R. C., Kaufman, Y. J., Tanre, D., Mattoo, S., Martins, J. V., Ichoku, C., Koren, I., Yu, H. B., and Holben, B. N.: Global aerosol climatology from the MODIS satellite sensors, *J. Geophys. Res.-Atmos.*, 113, D14S07, doi:10.1029/2007jd009661, 2008.

Rogers, R. R. and Yau, M. K.: *A short course in cloud physics*, 125–126 pp., 1989.

Russell, L. M., Hawkins, L. N., Frossard, A. A., Quinn, P. K., and Bates, T. S.: Carbohydrate-like composition of submicron atmospheric particles and their production from ocean bubble bursting, *P. Natl. Acad. Sci. USA*, 107, 6652–6657, doi:10.1073/pnas.0908905107, 2010.

Shaw, W. J., Allwine, K. J., Fritz, B. G., Rutz, F. C., Rishel, J. P., and Chapman, E. G.: Evaluation of the wind erosion module in DUSTRAN, *Atmos. Environ.*, 42, 1907–1921, doi:10.1016/j.atmosenv.2007.11.022, 2008.

Shrivastava, M., Fast, J., Easter, R., Jr., W. I. G., Zaveri, R. A., Jimenez, J. L., Saide, P., and Hodzic, A.: Modeling organic aerosols in a megacity: comparison of simple and complex representations of the volatility basis set approach, *Atmos. Chem. Phys. Discuss.*, 10, 30205–30277, doi:10.5194/acpd-10-30205-2010, 2010.

Skamarock, W. C.: Evaluating mesoscale NWP models using kinetic energy spectra, *Mon. Weather Rev.*, 132, 3019–3032, 2004.

Stevens, B., Vali, G., Comstock, K., Wood, R., van Zanten, M. C., Austin, P. H., Bretherton, C. S., and Lenschow, D. H.: Pockets of open cells and drizzle in marine stratocumulus, *B. Am. Meteorol. Soc.*, 86, 51, doi:10.1175/BAMS-86-1-51, 2005.

Stevens, B. and Feingold, G.: Untangling aerosol effects on clouds and precipitation in a buffered system, *Nature*, 461, 607–613, doi:10.1038/nature08281, 2009.

Toniazzo, T., Abel, S. J., Wood, R., Mechoso, C. R., Allen, G., and Shaffrey, L. C.: Large-scale and synoptic meteorology in the south-east Pacific during the observations campaign

## Assessing regional scale predictions of marine stratocumulus

Q. Yang et al.

Title Page

Abstract

Introduction

Conclusions

References

Tables

Figures

◀

▶

◀

▶

Back

Close

Full Screen / Esc

Printer-friendly Version

Interactive Discussion

VOCALS-REx in austral spring 2008, *Atmos. Chem. Phys.*, 11, 4977–5009, doi:10.5194/acp-11-4977-2011, 2011.

Twomey, S.: Influence of Pollution on Shortwave Albedo of Clouds, *J. Atmos. Sci.*, 34, 1149–1152, 1977.

5 Wang, H. and Feingold, G.: Modeling Mesoscale Cellular Structures and Drizzle in Marine Stratocumulus. Part I: Impact of Drizzle on the Formation and Evolution of Open Cells, *J. Atmos. Sci.*, 66, 3237–3256, doi:10.1175/2009jas3022.1, 2009a.

Wang, H. and Feingold, G.: Modeling Mesoscale Cellular Structures and Drizzle in Marine Stratocumulus. Part II: The Microphysics and Dynamics of the Boundary Region between  
10 Open and Closed Cells, *J. Atmos. Sci.*, 66, 3257–3275, doi:10.1175/2009jas3120.1, 2009b.

Wang, H., Skamarock, W. C., and Feingold, G.: Evaluation of Scalar Advection Schemes in the Advanced Research WRF Model Using Large-Eddy Simulations of Aerosol-Cloud Interactions, *Mon. Weather Rev.*, 137, 2547–2558, doi:10.1175/2009mwr2820.1, 2009.

15 Wiedinmyer, C., Akagi, S. K., Yokelson, R. J., Emmons, L. K., Al-Saadi, J. A., Orlando, J. J., and Soja, A. J.: The Fire INventory from NCAR (FINN) – a high resolution global model to estimate the emissions from open burning, *Geosci. Model Dev. Discuss.*, 3, 2439–2476, doi:10.5194/gmdd-3-2439-2010, 2010.

Wood, R. and Bretherton, C. S.: Boundary layer depth, entrainment, and decoupling in the cloud-capped subtropical and tropical marine boundary layer, *J. Climate.*, 17, 3576–3588, 2004.

20 Wood, R., Bretherton, C. S., Leon, D., Clarke, A. D., Zuidema, P., Allen, G., and Coe, H.: An aircraft case study of the spatial transition from closed to open mesoscale cellular convection over the Southeast Pacific, *Atmos. Chem. Phys.*, 11, 2341–2370, doi:10.5194/acp-11-2341-2011, 2011a.

25 Wood, R., Mechoso, C. R., Bretherton, C. S., Weller, R. A., Huebert, B., Straneo, F., Albrecht, B. A., Coe, H., Allen, G., Vaughan, G., Daum, P., Fairall, C., Chand, D., Klenner, L. G., Garreaud, R., Grados, C., Covert, D. S., Bates, T. S., Krejci, R., Russell, L. M., de Szoeko, S., Brewer, A., Yuter, S. E., Springston, S. R., Chaigneau, A., Toniazzo, T., Minnis, P., Palikonda, R., Abel, S. J., Brown, W. O. J., Williams, S., Fochesatto, J., Brioude, J., and Bower, K. N.: The VAMOS Ocean-Cloud-Atmosphere-Land Study Regional Experiment (VOCALS-REx): goals, platforms, and field operations, *Atmos. Chem. Phys.*, 11, 627–654, doi:10.5194/acp-11-627-2011, 2011b.

30 Wyant, M. C., Wood, R., Bretherton, C. S., Mechoso, C. R., Bacmeister, J., Balmaseda, M. A.,

**Assessing regional  
scale predictions of  
marine  
stratocumulus**

Q. Yang et al.

[Title Page](#)[Abstract](#)[Introduction](#)[Conclusions](#)[References](#)[Tables](#)[Figures](#)[⏪](#)[⏩](#)[◀](#)[▶](#)[Back](#)[Close](#)[Full Screen / Esc](#)[Printer-friendly Version](#)[Interactive Discussion](#)

Barrett, B., Codron, F., Earnshaw, P., Fast, J., Hannay, C., Kaiser, J. W., Kitagawa, H., Klein, S. A., Kohler, M., Manganello, J., Pan, H. L., Sun, F., Wang, S., and Wang, Y.: The PreVOCA experiment: modeling the lower troposphere in the Southeast Pacific, *Atmos. Chem. Phys.*, 10, 4757–4774, doi:10.5194/acp-10-4757-2010, 2010.

5 Yang, M., Blomquist, B. W., and Huebert, B. J.: Constraining the concentration of the hydroxyl radical in a stratocumulus-topped marine boundary layer from sea-to-air eddy covariance flux measurements of dimethylsulfide, *Atmos. Chem. Phys.*, 9, 9225–9236, doi:10.5194/acp-9-9225-2009, 2009.

10 Zaveri, R. A., Easter, R. C., Fast, J. D., and Peters, L. K.: Model for Simulating Aerosol Interactions and Chemistry (MOSAIC), *J. Geophys. Res.-Atmos.*, 113, D13204, doi:10.1029/2007jd008782, 2008.

Zhang, Y., Olsen, S. C., and Dubey, M. K.: WRF/Chem simulated springtime impact of rising Asian emissions on air quality over the U. S., *Atmos. Environ.*, 44, 2799–2812, doi:10.1016/j.atmosenv.2010.05.003, 2010.

15 Zhao, C., Liu, X., Leung, L. R., Johnson, B., McFarlane, S. A., Gustafson, W. I., Fast, J. D., and Easter, R.: The spatial distribution of mineral dust and its shortwave radiative forcing over North Africa: modeling sensitivities to dust emissions and aerosol size treatments, *Atmos. Chem. Phys.*, 10, 8821–8838, doi:10.5194/acp-10-8821-2010, 2010.

20 Zuidema, P., Painemal, D., de Szoeko, S., and Fairall, C.: Stratocumulus Cloud-Top Height Estimates and Their Climatic Implications, *J. Climate*, 22, 4652–4666, doi:10.1175/2009jcli2708.1, 2009.

## Assessing regional scale predictions of marine stratocumulus

Q. Yang et al.

Title Page

Abstract

Introduction

Conclusions

References

Tables

Figures

⏪

⏩

◀

▶

Back

Close

Full Screen / Esc

Printer-friendly Version

Interactive Discussion



**Table 1.** Primary model configuration settings.

Atmospheric Process	WRF Option
Tracer advection	Monotonic
Longwave radiation	RRTM
Shortwave radiation	Goddard
Surface layer	MM5 similarity theory
Land surface	Noah
Boundary layer	YSU
Deep and shallow cumulus clouds	Turned off
Cloud microphysics	Morrison
Gas phase chemistry	CBM-Z with DMS reactions
Aerosol chemistry	8-bin MOSAIC (for AERO)
Photolysis	Madronich (for AERO)
Aerosol direct & semi-direct effects	Turned on (for AERO)
Aqueous chemistry, wet scavenging, and cloud-aerosol interactions	Turned on (for AERO)

**Assessing regional  
scale predictions of  
marine  
stratocumulus**

Q. Yang et al.

[Title Page](#)[Abstract](#)[Introduction](#)[Conclusions](#)[References](#)[Tables](#)[Figures](#)[⏪](#)[⏩](#)[◀](#)[▶](#)[Back](#)[Close](#)[Full Screen / Esc](#)[Printer-friendly Version](#)[Interactive Discussion](#)

**Table 2.** Particle dry-diameter range for the eight MOSAIC aerosol size bins employed in this study.

Bin	Lower Diameter ( $\mu\text{m}$ )	Upper Diameter ( $\mu\text{m}$ )
1	0.0390625	0.078125
2	0.078125	0.15625
3	0.15625	0.3125
4	0.3125	0.625
5	0.625	1.25
6	1.25	2.5
7	2.5	5.0
8	5.0	10.0

**Table 3.** Observed and simulated MBL temperature and humidity, 10-m wind speed, SST, and boundary layer height.

Variable (Units)	Platform/ Simulations	Coastal region <sup>b</sup> Mean/Std	Remote region <sup>b</sup> Mean/Std	Both regions Mean/Std
Temperature, humidity, and MBLH				
$\theta_v$ (K) <sup>a</sup>	RB	290.5/0.8	292.7/3.1	291.9/2.7
	AERO	289.7/1.3	290.7/0.7	290.3/1.1
	MET	290.1/1.2	290.9/0.6	290.5/1.1
$q_v$ (g kg <sup>-1</sup> ) <sup>a</sup>	RB	7.6/0.7	9.4/2.4	8.7/2.1
	AERO	8.2/0.8	8.5/0.7	8.4/0.8
	MET	8.2/0.8	8.0/0.7	8.1/0.8
$d\theta_v/dh$ (K km <sup>-1</sup> )	RB	40.0	16.2	–
	AERO	32.4	18.6	–
	MET	21.1	23.7	–
$dq_v/dh$ (g kg <sup>-1</sup> km <sup>-1</sup> )	RB	–17.1	–10.7	–
	AERO	–9.0	–12.5	–
	MET	–5.0	–12.0	–
MBLH (m)	RB	1257/144	1445/98	1360/152
	AERO	1090/118	1377/187	1248/214
	MET	1189/151	1588/217	1408/276
Winds, SST				
$U_{10}$ (m s <sup>-1</sup> )	RB	4.8/1.3	8.2/1.3	6.2/2.1
	AERO	4.9/1.6	8.8/1.1	6.4/2.4
	MET	4.8/1.4	8.8/1.2	6.4/2.3
SST (°C)	RB	18.0/0.9	18.5/0.6	18.2/0.8
	AERO	17.7/0.5	18.5/0.5	18.1/0.6
	MET	17.7/0.5	18.5/0.5	18.1/0.6
Accumulation mode aerosol (0.156–2.69 μm) concentration				
$N_a$ (cm <sup>-3</sup> )	C-130	243/147	105/95	184/144
	AERO	160/68	81/36	126/68
Droplet number concentration				
$N_d$ (cm <sup>-3</sup> )	RB	203/84	85/55	154/93
	AERO	160/94	75/56	124/90
DMS transfer velocity ( $K_w$ ), DMS and SO <sub>2</sub> air concentrations				
$K_w$ (cm hr <sup>-1</sup> )	RB	3.80/1.96	9.04/2.95	5.69/3.44
	AERO	6.29/3.53	15.85/3.76	9.73/5.85
DMS Air (pptv)	RB	43.2/27.5	78.2/21.6	56.9/30.6
	AERO	138.4/49.6	216.5/41.0	169.1/60.1
SO <sub>2</sub> air (pptv)	RB	62.6/180.8	35.5/69.8	51.0/151.1
	AERO	49.1/144.7	8.6/18.6	31.7/111.8

<sup>a</sup> For below inversion base.

<sup>b</sup> Coastal and remote regions are defined as east and west of 78° W within the model domain, respectively.

**Assessing regional scale predictions of marine stratocumulus**

Q. Yang et al.

Title Page

Abstract

Introduction

Conclusions

References

Tables

Figures

◀

▶

◀

▶

Back

Close

Full Screen / Esc

Printer-friendly Version

Interactive Discussion



**Table 4.** Observed and simulated MBL submicron and supermicron aerosol composition.

Aerosol	Platform (instrument)/ Simulations	Diameter ( $\mu\text{m}$ )	Coastal region <sup>a</sup> Mean/Std ( $\mu\text{g m}^{-3}$ )	Remote region <sup>a</sup> Mean/Std ( $\mu\text{g m}^{-3}$ )	Both regions Mean/Std ( $\mu\text{g m}^{-3}$ )
Sulfate	C-130 (AMS) AERO	0.05–0.5	0.85/1.12 0.72/0.72	0.27/0.33 0.16/0.11	0.63/0.95 0.50/0.63
	RB (AMS) AERO	0.06–1.0	1.13/0.85 0.71/0.40	0.39/0.26 0.15/0.08	0.87/0.79 0.51/0.42
	G-1 (AMS) AERO	0.06–0.6	0.94/0.88 1.68/1.29	– –	– –
	G-1 (PILS) AERO	0.06–1.5	1.16/0.96 1.59/1.05	– –	– –
	RB (IC) AERO	< 1.1	1.08/0.95 0.76/0.36	0.31/0.15 0.20/0.15	0.76/0.82 0.53/0.40
	RB (IC) AERO	1.1–10	0.53/0.14 0.41/0.17	0.59/0.16 0.12/0.07	0.55/0.15 0.29/0.20
	C-130 (AMS) AERO	0.05–0.5	0.13/0.24 0.07/0.07	0.03/0.08 0.01/0.02	0.09/0.20 0.05/0.06
	RB (AMS) AERO	0.06–1.0	0.30/0.12 0.09/0.05	0.20/0.04 0.01/0.01	0.28/0.11 0.08/0.06
	G-1 (AMS) AERO	0.06–0.6	0.10/0.09 0.12/0.05	– –	– –
	RB (IC) AERO	< 1.1	0.23/0.17 0.08/0.06	0.07/0.04 0.01/0.02	0.16/0.15 0.05/0.06
Organics	C-130 (AMS) AERO	0.05–0.5	0.19/0.47 0.13/0.10	0.08/0.14 0.04/0.03	0.14/0.39 0.10/0.10
	RB (AMS) AERO	0.06–1.0	0.32/0.13 0.14/0.07	0.25/0.07 0.03/0.02	0.29/0.12 0.11/0.08
	G-1 (AMS) AERO	0.06–0.6	0.20/0.07 0.15/0.17	– –	– –
Chloride	G1 (PILS) AERO	0.06–1.5	0.24/0.37 0.29/0.23	– –	– –
	RB (IC) AERO	< 1.1	0.03/0.02 0.02/0.03	0.06/0.02 0.11/0.05	0.04/0.02 0.06/0.06
	RB (IC) AERO	1.1–10	3.02/1.14 6.25/2.23	4.18/1.27 8.81/2.70	3.41/1.34 7.19/2.72
	G1 (PILS) AERO	0.06–1.5	0.40/0.31 0.54/0.22	– –	– –
Sodium	RB (IC) AERO	< 1.1	0.07/0.02 0.14/0.04	0.06/0.02 0.14/0.04	0.07/0.02 0.14/0.04
	RB (IC) AERO	1.1–10	1.80/0.57 4.23/1.42	2.35/0.69 5.78/1.77	2.02/0.66 4.87/1.71

<sup>a</sup> Coastal and remote regions are defined as east and west of 78° W within the model domain, respectively.

**Assessing regional scale predictions of marine stratocumulus**

Q. Yang et al.

Title Page

Abstract Introduction

Conclusions References

Tables Figures

⏪ ⏩

◀ ▶

Back Close

Full Screen / Esc

Printer-friendly Version

Interactive Discussion



## Assessing regional scale predictions of marine stratocumulus

Q. Yang et al.

Title Page

Abstract

Introduction

Conclusions

References

Tables

Figures

◀

▶

◀

▶

Back

Close

Full Screen / Esc

Printer-friendly Version

Interactive Discussion



**Table 5.** Observed and simulated cloud properties.

Variable (Units)	Platform/ Simulations	Coastal region <sup>a</sup> Mean/Std	Remote region <sup>a</sup> Mean/Std	Both regions Mean/Std
Effective radius, cloud water path, and cloud optical thickness				
$r_e$ ( $\mu\text{m}$ )	MODIS Aqua	11.3/2.2	14.5/2.0	13.4/2.6
	AERO	10.5/1.1	12.6/1.7	11.9/1.8
	MET	8.5/0.6	8.5/0.6	8.5/0.6
CWP ( $\text{g m}^{-2}$ )	MODIS Aqua	79.2/23.1	99.2/20.1	92.8/23.1
	AERO	83.2/32.5	70.5/22.5	74.6/26.8
	MET	100.4/40.4	115.7/42.9	110.8/42.7
COT	MODIS Aqua	10.6/2.3	10.4/1.8	10.4/2.0
	AERO	17.7/6.5	11.9/3.7	13.8/5.5
	MET	19.2/7.6	21.9/8.0	21.0/8.0
Cloud fraction, cloud base and cloud thickness				
Daytime CF (%)	MODIS Aqua	73.7/10.8	76.4/5.6	75.4/8.2
	AERO	79.1/8.2	69.5/6.5	73.3/8.6
	MET	79.4/8.2	73.9/5.5	76.1/7.2
Nighttime CF (%)	MODIS Aqua	86.5/8.5	87.3/5.0	87.0/6.7
	AERO	89.4/7.3	80.3/5.0	84.0/7.9
	MET	88.9/7.3	84.2/5.5	86.1/6.7
Cloud base height (m)	C-130	867	1090	991
	AERO	869	1079	984
	MET	771	1075	941
Cloud thickness (m)	C-130	280	390	341
	AERO	281	391	341
	MET	293	429	369

<sup>a</sup> Coastal and remote regions are defined as east and west of 78° W within the model domain, respectively.

**Table 6.** Observed and simulated top-of-atmosphere (TOA) outgoing shortwave radiation and surface fluxes.

Variable (Units)	Platform/ Simulations	Coastal region <sup>a</sup> Mean/Std	Remote region <sup>a</sup> Mean/Std	Both regions Mean/Std
TOA outgoing fluxes				
TOA SW (W m <sup>-2</sup> )	MODIS Terra	360.8/69.6	341.2/52.5	347.5/59.2
	AERO	410.4/90.8	318.6/61.9	348.1/84.2
	MET	395.8/90.9	376.9/70.8	383.0/78.3
Surface fluxes				
Sensible heat (W m <sup>-2</sup> )	RB	3.0/3.2	6.1/6.5	4.1/4.9
	AERO	9.6/4.5	15.1/6.7	11.6/6.0
	MET	7.4/3.5	10.3/5.6	8.5/4.6
Latent heat (W m <sup>-2</sup> )	RB	76.5/23.9	115.5/30.5	90.7/32.4
	AERO	76.6/25.2	140.7/34.7	100.0/42.4
	MET	76.7/23.4	149.1/39.7	103.1/46.2
SW↓ <sup>b</sup> (W m <sup>-2</sup> )	RB	261.5/362.4	227.3/311.8	239.8/331.5
	AERO	257.0/356.8	209.5/295.1	226.8/319.7
	MET	222.3/336.0	238.2/323.9	232.4/328.4
LW↓ <sup>b</sup> (W m <sup>-2</sup> )	RB	373.7/21.4	364.9/25.6	370.2/23.5
	AERO	376.0/17.9	362.5/29.1	371.1/23.6
	MET	375.2/18.2	367.3/27.0	372.3/22.2

<sup>a</sup> Coastal and remote regions are defined as east and west of 78°W within the model domain, respectively.

<sup>b</sup> Downward fluxes.

**Assessing regional  
scale predictions of  
marine  
stratocumulus**

Q. Yang et al.

Title Page

Abstract

Introduction

Conclusions

References

Tables

Figures

⏪

⏩

◀

▶

Back

Close

Full Screen / Esc

Printer-friendly Version

Interactive Discussion



## Assessing regional scale predictions of marine stratocumulus

Q. Yang et al.

**Table 7.** Observed and simulated in-cloud and near-surface rain rates.

Regions (Units)	Platform/ Simulations	Coastal region <sup>a</sup> Mean/Median	Remote region <sup>a</sup> Mean/Median	Both Regions Mean/Median
In-cloud (mm day <sup>-1</sup> )	C-130	0.668/0.112	6.891/0.396	3.704/0.161
	AERO	0.037/0.013	0.163/0.052	0.099/0.019
	MET	0.012/0.004	0.052/0.013	0.031/0.006
Near surface (mm day <sup>-1</sup> )	C-130	0.001/ 0.000	5.175/0.002	3.619/0.000
	AERO	0.037/0.033	0.069/0.053	0.052/0.042
	MET	0.023/0.018	0.059/0.044	0.040/0.027

<sup>a</sup> Coastal and remote regions are defined as east and west of 78°W within the model domain, respectively.

Title Page

Abstract

Introduction

Conclusions

References

Tables

Figures

⏪

⏩

◀

▶

Back

Close

Full Screen / Esc

Printer-friendly Version

Interactive Discussion



## Assessing regional scale predictions of marine stratocumulus

Q. Yang et al.

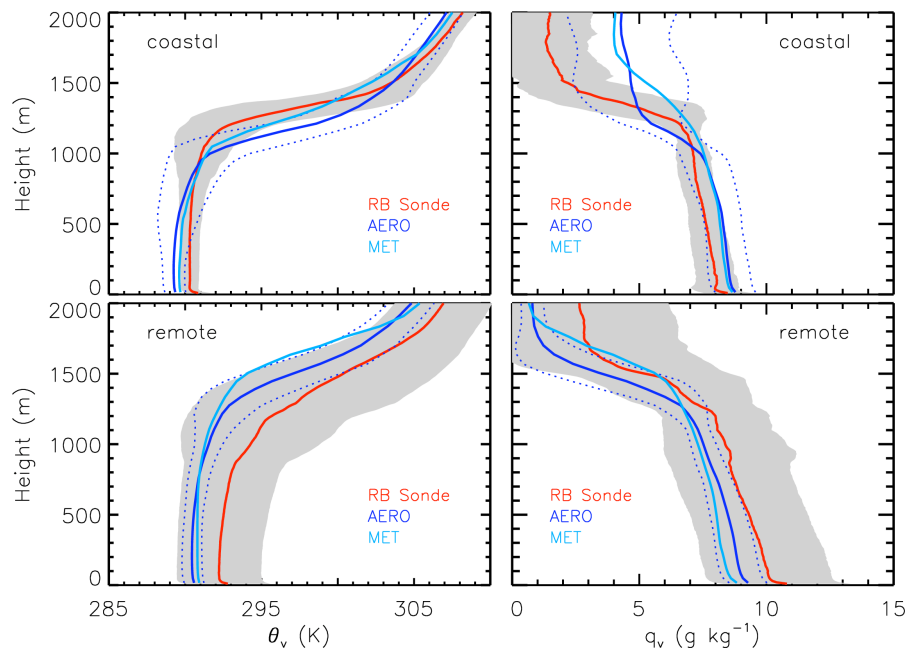


**Fig. 1.** Vertical profiles of virtual potential temperature ( $\theta_v$ ) and water vapor mixing ratio ( $q_v$ ) measured by radiosondes released from the RB ship and those from AERO (blue) and MET (light blue) simulations. The shaded area represents  $\pm 1\sigma$  of the observations. The dash blue lines also indicate the  $\pm 1\sigma$  of the AERO simulations.

[Title Page](#)
[Abstract](#)
[Introduction](#)
[Conclusions](#)
[References](#)
[Tables](#)
[Figures](#)
[⏪](#)
[⏩](#)
[◀](#)
[▶](#)
[Back](#)
[Close](#)
[Full Screen / Esc](#)
[Printer-friendly Version](#)
[Interactive Discussion](#)

**Assessing regional  
scale predictions of  
marine  
stratocumulus**

Q. Yang et al.

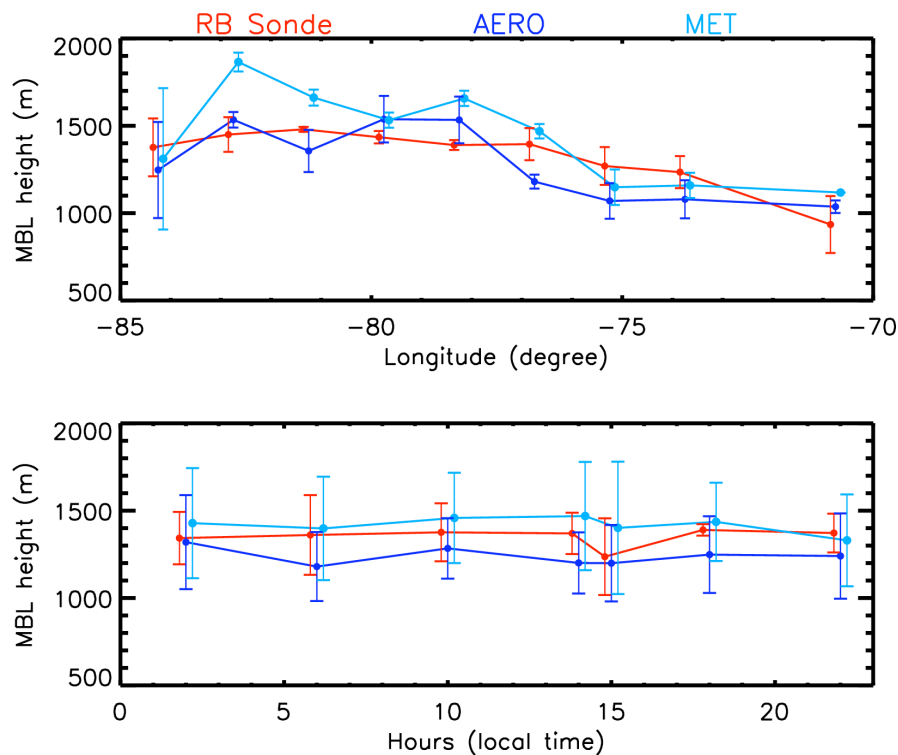


**Fig. 2.** Longitudinal and diurnal variations of the MBL heights derived from RB radiosondes measurements (red), and from the AERO (blue) and MET (light blue) simulations. The MBL heights are determined from temperature profiles in combination with humidity profiles.

[Title Page](#)[Abstract](#)[Introduction](#)[Conclusions](#)[References](#)[Tables](#)[Figures](#)[◀](#)[▶](#)[◀](#)[▶](#)[Back](#)[Close](#)[Full Screen / Esc](#)[Printer-friendly Version](#)[Interactive Discussion](#)

**Assessing regional  
scale predictions of  
marine  
stratocumulus**

Q. Yang et al.

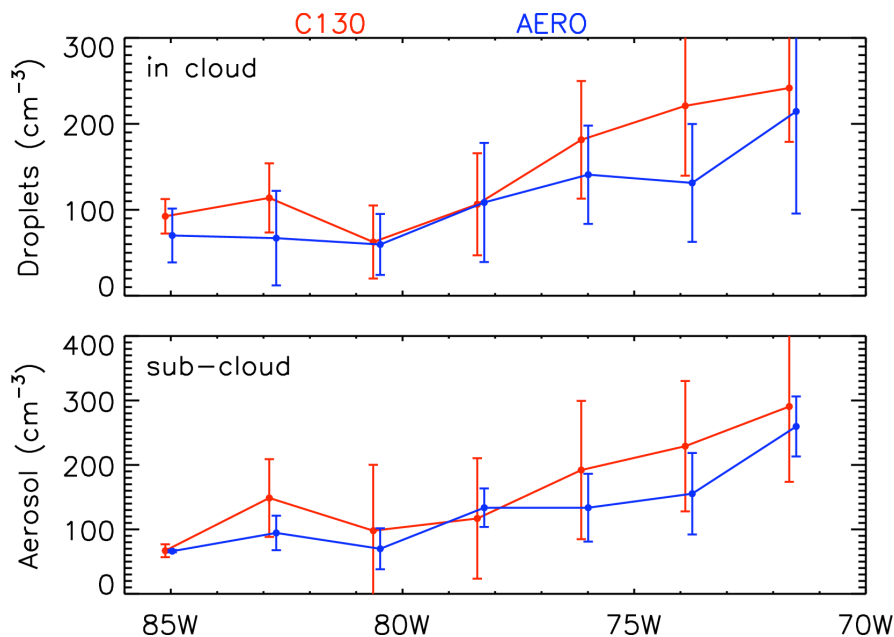


**Fig. 3.** Droplet number concentrations in the cloud layer and aerosol number concentrations in the sub-cloud layer observed on the C-130 aircraft (red) and predicted by the AERO simulation, (blue). The aerosol size range is 0.156–2.69  $\mu\text{m}$  in diameter for observations and 0.156–2.5  $\mu\text{m}$  for the model. The error bar represents  $\pm 1\sigma$ .

[Title Page](#)[Abstract](#)[Introduction](#)[Conclusions](#)[References](#)[Tables](#)[Figures](#)[◀](#)[▶](#)[◀](#)[▶](#)[Back](#)[Close](#)[Full Screen / Esc](#)[Printer-friendly Version](#)[Interactive Discussion](#)

**Assessing regional scale predictions of marine stratocumulus**

Q. Yang et al.

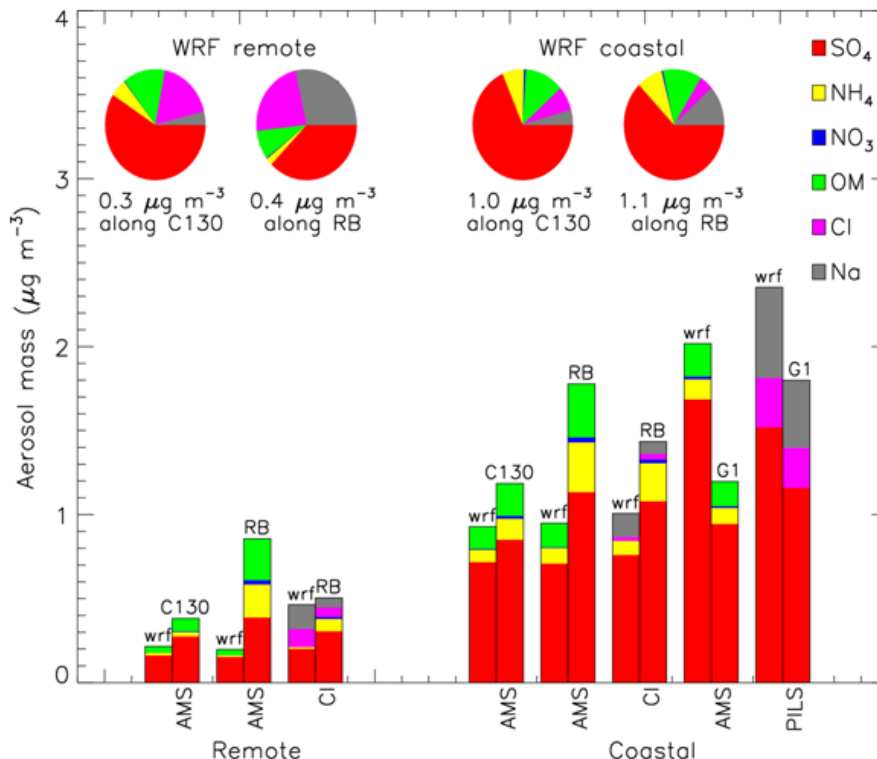


**Fig. 4.** MBL submicron aerosol mass composition from VOCALS-REx measurements and from the AERO simulation. The measurements are provided by AMS instruments onboard the C-130, RB, and G-1 and those sampled by the CIs and a PILS onboard the RB and G-1, respectively. The pie charts and the total aerosol mass provided below them are based on the AERO simulation; only data along C-130 and RB tracks at the sampling time are included into the calculations.

Title Page

Abstract Introduction

Conclusions References

Tables Figures

⏪ ⏩

◀ ▶

Back Close

Full Screen / Esc

Printer-friendly Version

Interactive Discussion



## Assessing regional scale predictions of marine stratocumulus

Q. Yang et al.

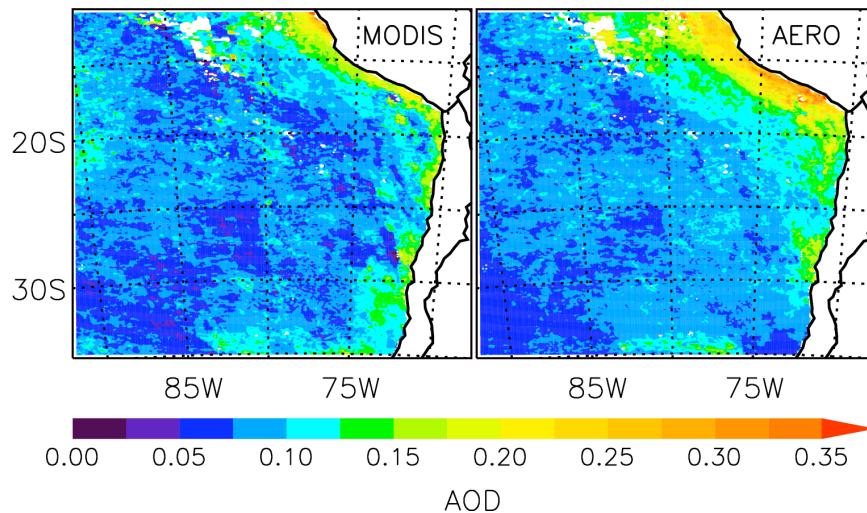


**Fig. 5.** AOD from MODIS (Aqua) measurements (left panel) and from the AERO simulation (right panel) during the VOCALS-REx period. Only model data at satellite scanning locations and times are included.

[Title Page](#)[Abstract](#)[Introduction](#)[Conclusions](#)[References](#)[Tables](#)[Figures](#)[◀](#)[▶](#)[◀](#)[▶](#)[Back](#)[Close](#)[Full Screen / Esc](#)[Printer-friendly Version](#)[Interactive Discussion](#)

**Assessing regional scale predictions of marine stratocumulus**

Q. Yang et al.

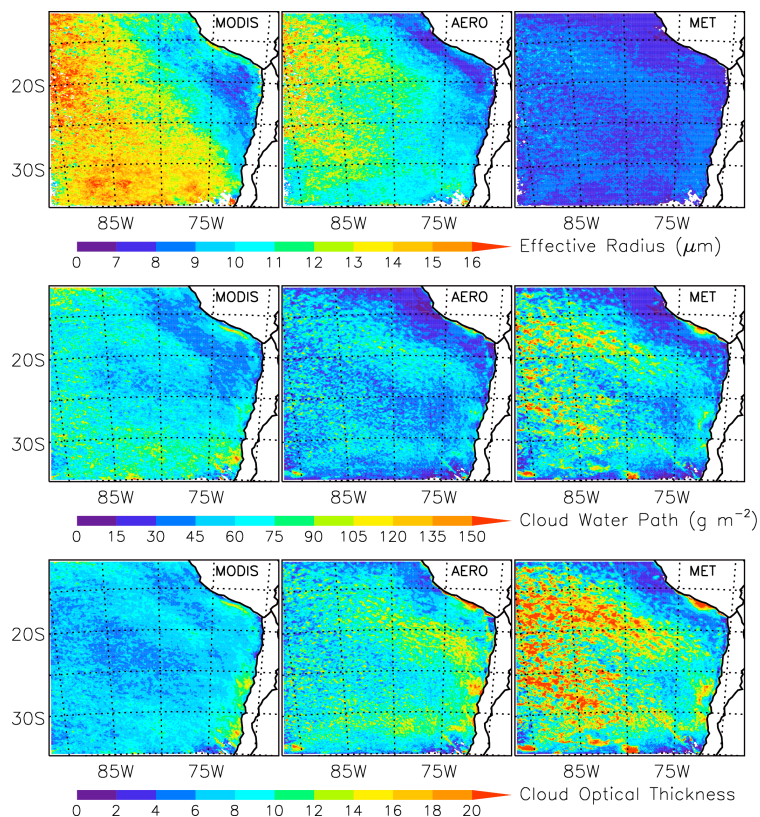


**Fig. 6.** Effective radius, cloud water path, and cloud optical thickness during the VOCALS-REX period from MODIS (Aqua) retrievals and from the AERO and MET simulations.

**Assessing regional  
scale predictions of  
marine  
stratocumulus**

Q. Yang et al.

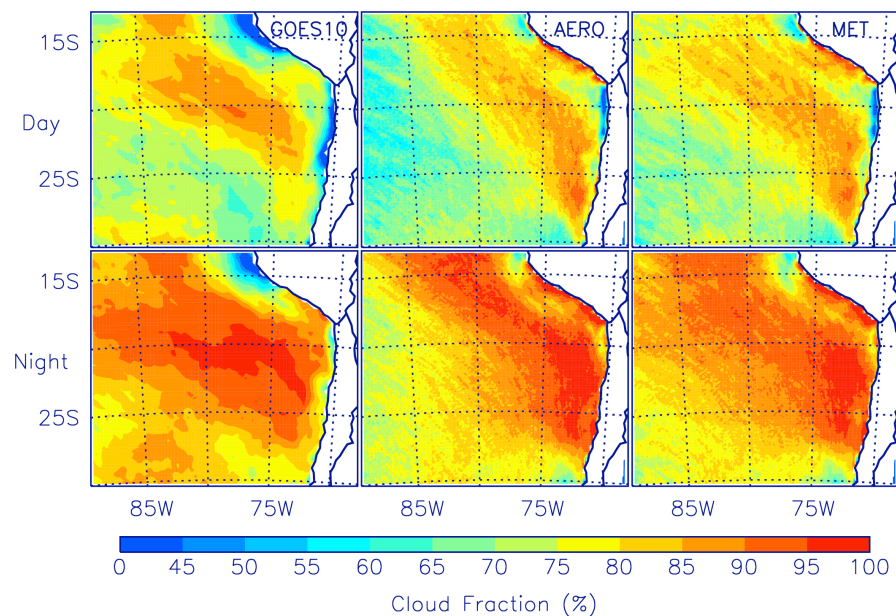


**Fig. 7.** Mean low cloud fractions during day and night for the VOCALS-REx period retrieved from GOES-10 (left), and those from the AERO (middle) and MET (right) model simulations.

Title Page

Abstract

Introduction

Conclusions

References

Tables

Figures

◀

▶

◀

▶

Back

Close

Full Screen / Esc

Printer-friendly Version

Interactive Discussion

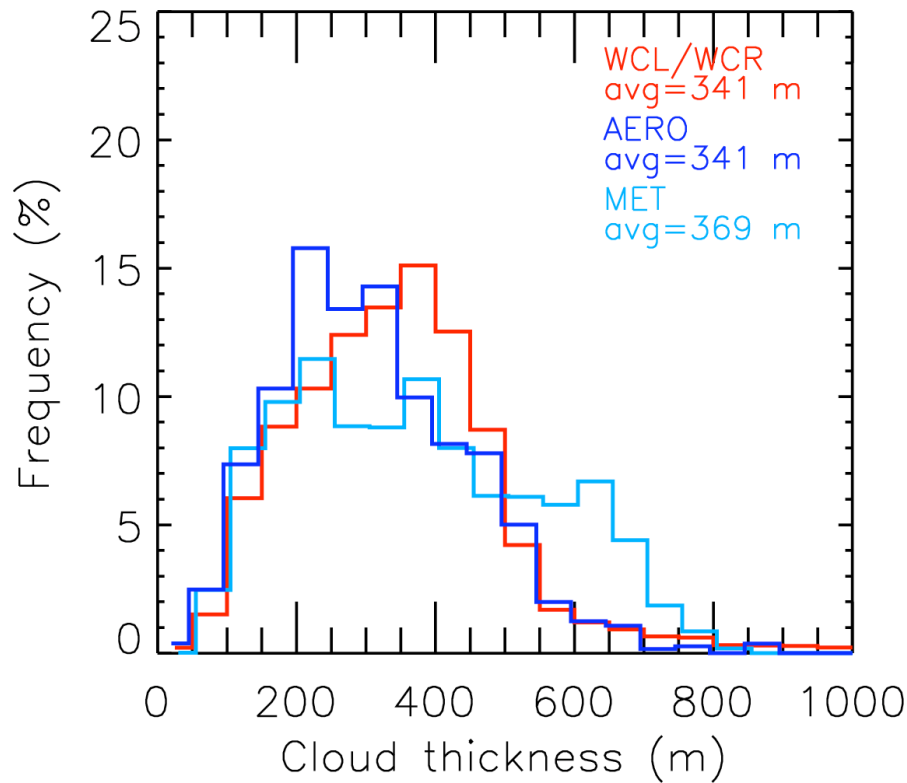


**Fig. 8.** Histogram of cloud thickness from the Wyoming cloud lidar (WCL) and radar (WCR) observations (red), and from the AERO (blue) and MET (light blue) simulations.

**Assessing regional scale predictions of marine stratocumulus**

Q. Yang et al.

Title Page	
Abstract	Introduction
Conclusions	References
Tables	Figures
◀	▶
◀	▶
Back	Close
Full Screen / Esc	
Printer-friendly Version	
Interactive Discussion	



**Assessing regional  
scale predictions of  
marine  
stratocumulus**

Q. Yang et al.

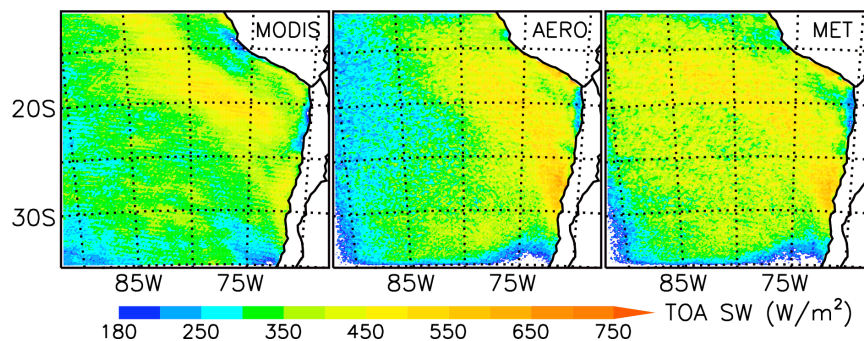


**Fig. 9.** Top of the atmosphere (TOA) outgoing shortwave (SW) radiation fluxes measured by CERES (Terra) and those simulated in the AERO and MET simulations.

[Title Page](#)[Abstract](#)[Introduction](#)[Conclusions](#)[References](#)[Tables](#)[Figures](#)[⏪](#)[⏩](#)[◀](#)[▶](#)[Back](#)[Close](#)[Full Screen / Esc](#)[Printer-friendly Version](#)[Interactive Discussion](#)

## Assessing regional scale predictions of marine stratocumulus

Q. Yang et al.

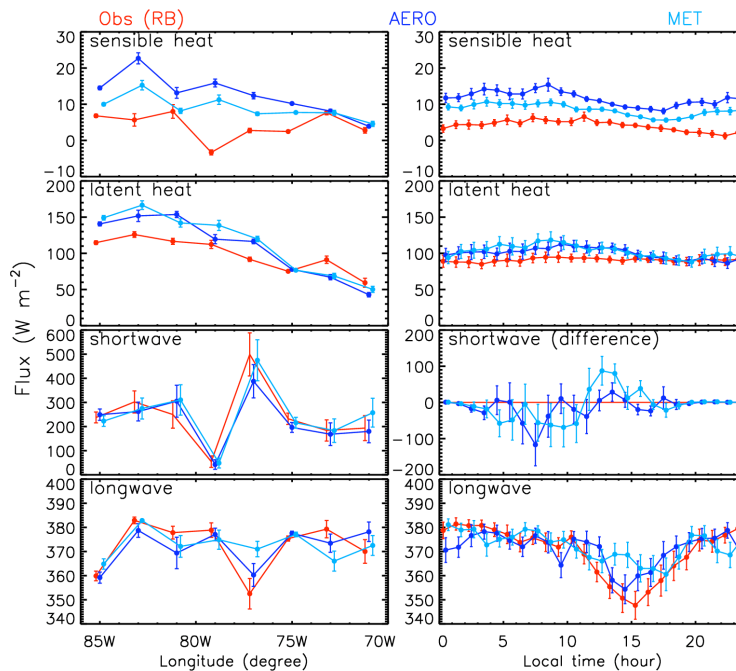


**Fig. 10.** Longitudinal and diurnal variations of surface fluxes including sensible heat, latent heat, downward shortwave, and downward longwave fluxes, from the sonic anemometer observations on the RB (red) and from the AERO (blue) and MET (light blue) simulations. The diurnal cycle of incoming shortwave fluxes is plotted as the difference between modeled and observed values. The vertical bars indicate  $\pm 2\sigma$ , where  $\sigma$  is the standard deviation of the mean value given by  $\sigma = \sqrt{\text{var}(x_i)/n}$ , where  $\text{var}(x_i)$  is the variance of data used for the averaging, and  $n$  is the number of the data points. Note that due to the large variability in some parameters,  $\sigma$  is not represented as the square root of the variance as in other figures.

Title Page

Abstract

Introduction

Conclusions

References

Tables

Figures

◀

▶

◀

▶

Back

Close

Full Screen / Esc

Printer-friendly Version

Interactive Discussion

## Assessing regional scale predictions of marine stratocumulus

Q. Yang et al.

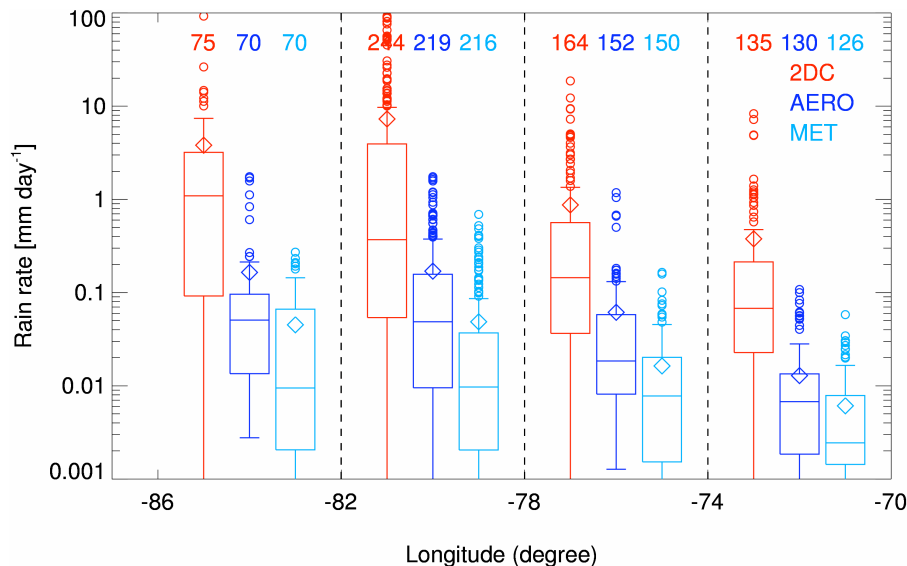


**Fig. 11.** Box and whisker plots of longitude-binned rain rates from in-cloud measurements (red) by a 2D-C probe onboard the C-130 aircraft and from corresponding in-cloud values in the AERO (blue) and MET (light blue) simulations. The bottom and top of the box are 25th and 75th percentiles. The median is shown inside the box. The 10th and 90th percentiles are shown by the dash outside the box. The open circles indicate outliers (lower than 10th or higher than 90th percentiles). The diamonds show the mean over all legs in each longitude bin. The numbers on the top indicate the number of data points used to produce the box and whisker plot.

Title Page	
Abstract	Introduction
Conclusions	References
Tables	Figures
◀	▶
◀	▶
Back	Close
Full Screen / Esc	
Printer-friendly Version	
Interactive Discussion	